Quantum metrology with multimode Gaussian states of multiple point sources

Xiao-Jun Liao and Yong-Qi Fu*
School of Physics, University of Electronic Science and Technology of China, Chengdu 611731, China

(Received 13 April 2022; accepted 19 July 2022; published 3 August 2022)

A unified theoretical framework is developed for measuring multimode Gaussian states of multiple point sources. The spatial and temporal mode functions are found analytically by aid of the circular symmetry of the object plane and aperture, as well as by the rectangular spectral density function of the background. They relate the modal operators and statistical moments to the locations of the point sources through the prolate spheroidal functions. An experimentally straightforward implementation is proposed, which consists of a nonabsorptive polarization- and phase-modulating spatial light modulator (SLM), three lenses, and a polarization beam splitter. Interestingly, it is found that the spatial modal annihilation operators are related to the modal field operators in the image plane by a simple complex-valued scale factor. The quantum Fisher information matrix and quantum Cramér-Rao bound (QCRB) are also discussed. The numerical calculation of QCRB is completed for the case where the spatially multimode aperture fields are prepared by the spatial propagation from temporally single-mode thermal states, coherent states, or quadrature squeezed states of the point sources in the object plane. The results show that the Rayleigh limit can always be surpassed by means of increasing the mean photon rate or the squeeze parameter.

DOI: 10.1103/PhysRevA.106.022602

I. INTRODUCTION

Modes and states are two fundamental aspects of classical and quantum optics, especially in understanding the resolution of any optical measurement in microscopy, astronomy, remote sensing, and many other fields of science and technology. As the modes are normalized solutions of Maxwell equations, traditional measurements based on mode discrimination inevitably suffer from diffraction effects, such as the well-known Rayleigh limit. On the contrary, quantum measurements based on quantum state discrimination have demonstrated that diffraction limits are irrelevant here, and that the ultimate bounds of the measurement are determined by the quantum properties of photons. Therefore, it is important to develop a quantum theory for the measurement of general multimode quantum states of multiple sources.

One-mode or two-mode quantum light was the focus of early research in quantum optics. Although quantum electrodynamics [1] and quantum coherence theory [2,3] treat light as a multimode field composed of many quantized harmonic oscillators, their specific applications were mainly devoted to one or two modes. This is especially true in the study of nonclassical states [4], including quantum state tomography [5–7], single-photon generation [8], preparation of entangled photon pairs using spontaneous parametric down conversion [4,9], four-wave mixing [10], quantum dots [11], and nitrogen vacancy defects [12]. In quantum metrology [13], one-mode or two-mode squeezed light or entangled photon pairs are utilized as probes to measure quantum systems and estimate their parameters. Prominent progress has been made recently in resolving two incoherent point sources [14–20]. But it is mainly about two-mode states, and is currently difficult to extend to multimode and multiple point sources.

Nonetheless, multimode quantum light has attracted much attention for superresolution reconstruction in one-dimensional (1D) [21,22] and two-dimensional (2D) [23,24] imaging, and more recently for understanding the intrinsic properties of light and applications in emerging technologies. The intrinsic properties include wave-particle duality and multipartite entanglement [25] with modal degrees of freedom, while the applications are aimed at mode-coupled quantum networks [26], quantum computing [27], and enhanced resolution in quantum metrology [25]. Thanks to the linearity of the evolution equations of the mode and state functions, any multimode quantum state can be represented as a linear combination of the mode basis and the state basis [25]. This "double linearity" makes multimode quantum states mathematically more tractable and physically easier to implement, as demonstrated in the generation [28], propagation [29], and detection processes [2]. Specifically, for quantum metrology, the above fact enables the optimization to find the optimal mode with the lowest quantum Cramér-Rao bound of the parameter uncertainty, in addition to the optimization to find the optimal quantum state of the probe light.

However, as mentioned previously, the measurement of multimode and multiple point sources remains difficult. Considering this, this paper deals with multimode Gaussian states of multiple point sources in a unified theoretical framework for imaging and metrology. Firstly, with the quantum diffraction integral [29] and the mutual coherence functions [30], the spatiotemporal mode functions of a circularly symmetrical

*yqfu@uestc.edu.cn

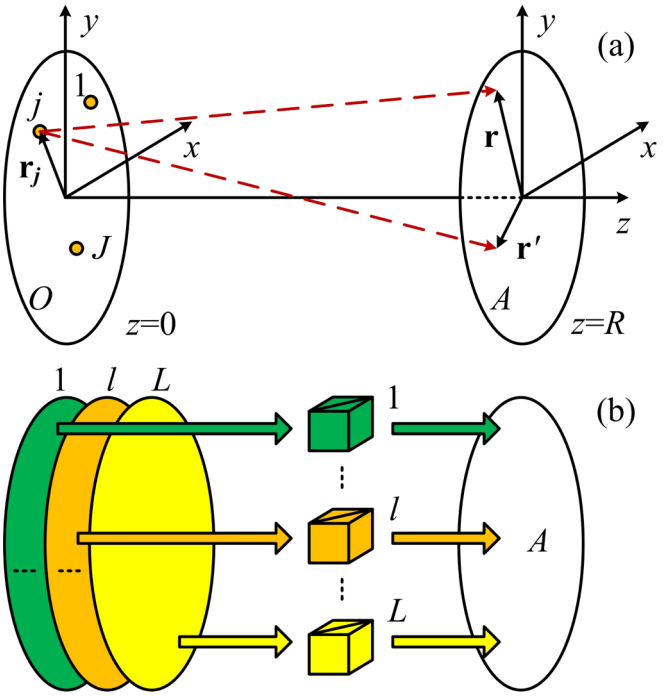

FIG. 1. (a) Quantum diffraction from a circular object plane O of radius b to a circular aperture A of radius a. The background is uniform, while the J point sources are independent of each other. (b) Mode channel model with beam splitters to account for modal losses. Each mode covers the entire circular areas of the object plane and the aperture, and the loss in each channel is described by a beam splitter along the propagation path.

optical system are found. The modal operators and coherency matrices are analytically expressed in terms of the prolate spheroidal functions [31,32]. Secondly, an experimentally straightforward implementation is proposed, which consists of a spatial light modulator (SLM), three lenses, a polarization beam splitter (PBS), and some further measurement devices, such as an array of photodetectors or homodyne detectors in the image plane. Finally, the quantum Fisher information matrix (QFIM) and quantum Cramér-Rao bound (QCRB) are connected to the displacement vectors, coherency matrices, and fluctuation-related matrices. The numerical calculation of the QCRB is also presented.

This paper proceeds as follows. In Sec. II, the theoretical framework is developed. Section III describes the implementation and image plane measurements. Section IV discusses the QFIM and QCRB. Concluding remarks are made in Sec. V.

II. THEORETICAL FRAMEWORK

A. System model and assumptions

Consider a background and J point sources located in an object plane O of radius b at $z = 0$, an optical instrument with an aperture A of radius a at $z = R$, and an image plane representing an array of photodetectors or homodyne detectors. The background and aperture are circularly symmetrical with respect to the z axis [see Fig. 1(a)]. The light radiated by the jth source and studied in the transverse plane at z is represented by the positive-frequency field operator $\hat{E}_{j,z}(\mathbf{r}, t)$, which is normalized such that $\hat{N}_{j,z} = \hat{E}^{\dagger}_{j,z}\hat{E}_{j,z}$ gives the photon flux operator in units of $1/(\mathrm{m}^2\,\mathrm{s})$, $\hat{I}_{j,z} = \hbar\omega\hat{N}_{j,z}$ gives the energy flux operator, and [30,33]

$$\Gamma_{j,z}(\mathbf{r}, \mathbf{r}'; t, t') = \hbar\omega\,\mathrm{Tr}[\hat{E}_{j,z}(\mathbf{r}', t')\hat{\rho}_j\hat{E}^{\dagger}_{j,z}(\mathbf{r}, t)] \tag{1}$$

gives the mutual coherence function [2]. In Eq. (1), $\hat{\rho}_j$ represents the density operator, $\hbar\omega$ is the photon energy, $j = 0$ indicates the background, and Tr denotes the trace of the following operators.

Note that throughout this paper the symbols with a subscript, e.g., $\hat{\rho}_j$, may denote a single quantity or all the quantities indexed by the subscript, which can be judged from the context without confusion.

The fields emitted by the sources are assumed to be statistically independent, quasimonochromatic, stationary in time, and in spectrally pure [33] Gaussian states. The field of the background is additionally uniform in the object plane. Moreover, for simplicity, a single linear polarization, the $+z$ propagating component of the field, and the paraxial approximation are considered.

Under these assumptions, in the object plane O and for the point sources [34], $j = 1, \ldots, J$,

$$\hat{E}_{j,O}(\mathbf{r}, t) = \mathcal{E}\hat{A}_{j,O}(t)e^{-i\omega_0 t}\delta(\mathbf{r} - \mathbf{r}_j), \tag{2}$$

$$\varphi_{j,O}(\mathbf{r}, \mathbf{r}') = \frac{\pi}{k_0^2}\hbar\omega_0\mathcal{N}_j\delta(\mathbf{r} - \mathbf{r}_j)\delta(\mathbf{r}' - \mathbf{r}), \tag{3}$$

$$\chi_j(t - t') = \frac{1}{\mathcal{N}_j}\mathrm{Tr}\big[\hat{A}_{j,O}(t')\hat{\rho}_j\hat{A}^{\dagger}_{j,O}(t)\big], \tag{4}$$

and for the background, $j = 0$,

$$N_{0,O}(\mathbf{r}) = N_0, \tag{5}$$

$$\varphi_{0,O}(\mathbf{r}, \mathbf{r}') = \frac{\pi}{k_0^2}\hbar\omega_0 N_0\delta(\mathbf{r}' - \mathbf{r}). \tag{6}$$

In the above equations, $\mathcal{E}$ accounts for several factors, including the single-photon electric field, Eq. (1), and the definition of the photon flux operator $\hat{N}_{j,O} = \hat{E}^{\dagger}_{j,O}\hat{E}_{j,O}$. The relation $\mathcal{E}^2 = \pi/k_0^2$ holds. $\hat{A}_{j,O}(t)$ is the slowly varying annihilation operator. ω_0 is the central angular frequency under the quasimonochromatic assumption. $k_0 = \omega_0/c$, and c is the speed of light in vacuum. The mutual coherence function $\Gamma_{j,O}(\mathbf{r}, \mathbf{r}'; t, t')$ factors into the spatial part $\varphi_{j,O}(\mathbf{r}, \mathbf{r}')$ and the temporal part $\chi_j(t - t')\exp[i\omega_0(t - t')]$ for the spectrally pure field. $\chi_j(t - t')$ is normalized such that $\chi_j(0) = 1$, and remains unchanged during propagation. $\mathcal{N}_j$ and $\pi b^2 N_0$ give the emitted mean photon rates.

B. Quantum diffraction

While $\chi_j(t - t')$ are determined only by the sources, $\varphi_{j,z}(\mathbf{r}, \mathbf{r}')$ vary along the propagation path and depend on the sources and the Green's function of free-space diffraction [29,34],

$$G(\mathbf{r}, z; t) = \delta(t)\frac{k_0}{i2\pi z}\exp\left[ik_0\left(z + \frac{|\mathbf{r}|^2}{2z}\right)\right], \tag{7}$$

from the object plane to a transverse plane at z. The aperture fields $\hat{E}_{j,A}(\mathbf{r},t)$ can be solved for through the quantum diffraction integral, which is essentially the spatiotemporal convolution integral of the source fields $\hat{E}_{j,O}(\mathbf{r},t)$ and the Green's function $G(\mathbf{r},R;t)$.

At the aperture, the field component originating from the jth point source can be written as either of the following equations,

$$\hat{E}_{j,A}(\mathbf{r},t)=\frac{\mathcal{E}\hat{A}_{j,O}(t)}{i\lambda_0 R}e^{-i\omega_0 t}e^{ik_0\left(R+|\mathbf{r}-\mathbf{r}_j|^2/2R\right)}, \tag{8}$$

$$\varphi_{j,A}(\mathbf{r},\mathbf{r}')=a_{j,A}e^{i(k_0/R)[(\mathbf{r}'^2-\mathbf{r}^2)/2+(\mathbf{r}-\mathbf{r}')\cdot\mathbf{r}_j]}, \tag{9}$$

where $a_{j,A}=\hbar\omega_0\mathcal{N}_j/4\pi R^2$. For the field component from the background, it is straightforward to use the van Cittert-Zernike theorem [33,35], which delivers

$$\varphi_{0,A}(\mathbf{r},\mathbf{r}')=a_{0,A}\exp[(i\pi/\lambda_0 R)(\mathbf{r}'^2-\mathbf{r}^2)]\times\int_O d^2\mathbf{r}''\exp[(ik_0/R)(\mathbf{r}-\mathbf{r}')\cdot\mathbf{r}''], \tag{10}$$

where $a_{0,A}=\hbar\omega_0 N_0/4\pi R^2$. This theorem follows directly from the Fresnel-Kirchhoff diffraction formula with paraxial approximation, and is equivalent to the quantum diffraction integral.

Since any spatiotemporally band-limited function can be expanded into a series by a set of spatiotemporal mode functions $\xi_p(\mathbf{r})\zeta_m(t)$, which are complete and orthonormal (CON) [36] over the aperture A and the observation interval $(0,T)$, the aperture field components can be expanded as

$$\hat{E}_{j,A}(\mathbf{r},t)=\sum_{p=0}^{P}\sum_{m=0}^{M}\hat{a}_{j,p,m}\xi_p(\mathbf{r})\zeta_m(t)e^{-i\omega_0 t}, \tag{11}$$

with $P,M\to\infty$. The modal annihilation operators

$$\hat{a}_{j,p,m}=\int_A\int_0^T\xi_p^*(\mathbf{r})\zeta_m^*(t)e^{i\omega_0 t}\hat{E}_{j,A}(\mathbf{r},t)d^2\mathbf{r}\,dt \tag{12}$$

obey the canonical commutation relations (CCRs)

$$[\hat{a}_{j,p,m},\hat{a}_{j,q,n}]=0,\quad [\hat{a}_{j,p,m},\hat{a}^\dagger_{j,q,n}]=\delta_{pq}\delta_{mn}. \tag{13}$$

When spatiotemporally band limited, $\hat{E}_{j,O}(\mathbf{r},t)$ can be similarly expanded, resulting in the modal annihilation operators $\hat{b}_{j,p,m}$. Of particular interest is the case where $\xi_p(\mathbf{r})$ are also CON over the object plane. In this case, $\hat{a}_{j,p,m}$ and $\hat{b}_{j,p,m}$ are related by the beam-splitter model [29],

$$\hat{a}_{j,p,m}=\sqrt{\eta_{p,m}}\hat{b}_{j,p,m}+\sqrt{1-\eta_{p,m}}\hat{e}_{j,p,m}, \tag{14}$$

where $\eta_{p,m}=\nu_p\gamma_m$, and ν_p and γ_m are the eigenvalues associated with $\xi_p(\mathbf{r})$ and $\zeta_m(t)$, respectively. $\hat{e}_{j,p,m}$ are the modal annihilation operators of the vacuum accounting for the excitation of the modes by the environment. $\hat{a}_{j,p,m}$ preserve the canonical commutator structure of $\hat{b}_{j,p,m}$. In this way, the spatiotemporal modes can be thought of as parallel channels with efficiencies $\eta_{p,m}<1$, which is a natural generalization of the beam-splitter loss model widely used in the single-mode situations. This parallel-channel model is illustrated in Fig. 1(b). Note that the two-element vector index $l=(p,m)$ is used to conveniently specify the entire spatiotemporal mode related to $\xi_p(\mathbf{r})\zeta_m(t)$, while p or m is used for an individual spatial or temporal part. There are $L=(P+1)\times(M+1)$ spatiotemporal modes in total. Since the vacuum does not contribute to the photon counting, $\hat{e}_{j,p,m}$ average to zeros in the photon measurements.

C. Multimode Gaussian density operators and coherency matrices

The multimode Gaussian density operator for the aperture field originating from the jth point source can be written in its P representation [3] as

$$\hat{\rho}_j=\pi^{-L}|\det\mathbf{V}_j|^{-1}\int e^{-\left(\mathbf{a}^\dagger-\langle\hat{\mathbf{a}}_j\rangle^\dagger\right)\mathbf{V}_j^{-1}\left(\mathbf{a}-\langle\hat{\mathbf{a}}_j\rangle\right)}|\mathbf{a}\rangle\langle\mathbf{a}|d^{2L}\mathbf{a}, \tag{15}$$

where $\hat{\mathbf{a}}_j$ is defined as an L-dimensional column vector of $\hat{a}_{j,p,m}$, and $\mathbf{V}_j$ is defined as an $L\times L$ coherency matrix of $V_{j,p,m,q,n}$,

$$\langle\hat{a}_{j,p,m}\rangle=\mathrm{Tr}(\hat{\rho}_j\hat{a}_{j,p,m}), \tag{16}$$

$$V_{j,p,m,q,n}=V^{(0)}_{j,p,m,q,n}-V^{(d)}_{j,p,m,q,n}, \tag{17}$$

$$V^{(0)}_{j,p,m,q,n}=\mathrm{Tr}(\hat{a}_{j,p,m}\hat{\rho}_j\hat{a}^\dagger_{j,q,n}), \tag{18}$$

$$V^{(d)}_{j,p,m,q,n}=\langle\hat{a}_{j,p,m}\rangle\langle\hat{a}_{j,q,n}\rangle^*. \tag{19}$$

Note the index transfers $l=(p,m)$ and $l'=(q,n)$, where $l,l'=1,\ldots,L$. Once $\langle\hat{\mathbf{a}}_j\rangle$ and $\mathbf{V}_j$ are determined, the matrix elements of $\hat{\rho}_j$ in an appropriate representation are also determined, which can be further used for state discrimination among multiple objects.

It is suggestive from Eq. (15) that the diagonalization of $\mathbf{V}_j^{-1}$ makes $\hat{\rho}_j$ factor into single-mode density operators $\hat{\rho}_{j,p,m}$, which simplifies the measurement and reconstruction process. The same idea has been introduced into the theory of two-hypothesis testing by Helstrom [33]. For this purpose, it is straightforward from Eqs. (1), (12), and (18) to show that [33]

$$V^{(0)}_{j,p,m,q,n}=(\hbar\omega_0)^{-1}I_{j,p,q}\,\Xi_{j,m,n}, \tag{20}$$

$$I_{j,p,q}=\int_A d^2\mathbf{r}'\int_A d^2\mathbf{r}\,\xi_p^*(\mathbf{r}')\xi_q(\mathbf{r})\varphi_{j,A}(\mathbf{r},\mathbf{r}'), \tag{21}$$

$$\Xi_{j,m,n}=\int_0^T dt'\int_0^T dt\,\zeta_m^*(t')\zeta_n(t)\chi_j(t-t'). \tag{22}$$

The spatial parts $I_{j,p,q}$ and temporal parts $\Xi_{j,m,n}$ can be found separately by the following eigenvalue problems [33]:

$$\nu_p\xi_p(\mathbf{r}')=\frac{1}{\hbar\omega_0\mathcal{N}_{j,A}}\int_A\varphi_{j,A}(\mathbf{r},\mathbf{r}')\xi_p(\mathbf{r})d^2\mathbf{r}, \tag{23}$$

$$\gamma_m\zeta_m(t')=\frac{1}{T}\int_0^T\chi_j(t-t')\zeta_m(t)dt, \tag{24}$$

and the eigenfunctions $\xi_p(\mathbf{r})$ and $\zeta_m(t)$ are CON over the aperture A and the observation interval $(0,T)$, respectively. The relations $\sum_p\nu_p=1$ and $\sum_m\gamma_m=1$ hold. $\mathcal{N}_{j,A}$ is the received mean photon rate originating from the jth source, and $\mathcal{N}_{0,A}=N_0(\pi ab)^2/4\pi R^2$. Thus $I_{j,p,q}=\hbar\omega_0\mathcal{N}_{j,A}\nu_p\delta_{pq}$, $\Xi_{j,m,n}=T\gamma_m\delta_{mn}$, and the elements of the coherency matrices

read

$$V^{(0)}_{j,p,m,q,n} = \mathcal{N}_{j,A} T \nu_p \gamma_m \delta_{pq} \delta_{mn}. \tag{25}$$

Clearly, $\mathbf{V}^{(0)}_j$ is diagonal, and $\mathcal{N}_{j,A}T$ is divided into the spatiotemporal mode channels proportionally to the mode eigenvalues $\eta_{p,m} = \nu_p \gamma_m$ with $\sum_{p,m} \eta_{p,m} = 1$.

However, when $\varphi_{j,A}(\mathbf{r}, \mathbf{r}')$ and $\chi_j(t - t')$ related to the jth source are used to solve for the mode functions $\xi_p(\mathbf{r})$ and $\zeta_m(t)$, *only* $\mathbf{V}^{(0)}_j$ corresponding to the jth field component is diagonalized. Therefore, for the case where common sets of mode functions $\xi_p(\mathbf{r})$ and $\zeta_m(t)$ are used simultaneously for all the fields from the background and J point sources, care must be taken to choose the mutual coherence functions to make the following procedures tractable, which will be discussed in the next section.

D. Explicit spatiotemporal mode functions

When $\varphi_{0,A}(\mathbf{r}, \mathbf{r}')$ in Eq. (10) is substituted into the eigenvalue problem in Eq. (23), the eigenfunctions $\xi_p(\mathbf{r})$ and eigenvalues ν_p are related [33,37] to the 2D prolate spheroidal functions $\psi_p(\mathbf{r}/a)$ and their corresponding eigenvalues λ_p, which were studied by Slepian [31] and Frieden [36]. The eigenfunctions read

$$\xi_p(\mathbf{r}) = \exp\Big(\frac{i\pi}{\lambda_0 R}\mathbf{r}^2\Big)\frac{\psi^*_p(\mathbf{r}/a)}{a\sqrt{z_p}}, \tag{26}$$

where $z_p = \int_{A_1} \psi^*_p(\mathbf{r})\psi_p(\mathbf{r}) d^2\mathbf{r}$ are the normalization coefficients over the unit-radius disk A_1. The eigenvalues are given by $\nu_p = 4\lambda_p/\beta^2$, and $p = (N, n)$ is the notational transfer of the mode indices. Thus $\xi_p(\mathbf{r})$ are CON over the aperture A, $|\mathbf{r}| \leqslant a$, and any 2D function band limited [31,36] by the space-bandwidth product $\beta = k_0 ab/R$ can be expanded by $\xi_p(\mathbf{r})$.

Similarly, when the spectral density function $X_j(\omega)$, i.e., the Fourier transform of $\chi_j(t - t')$, is rectangular [33] with a bandwidth W,

$$X_j(\omega) = W^{-1} \quad (|\omega| < \pi W), \tag{27}$$

the eigenfunctions $\zeta_m(t)$ and eigenvalues γ_m of Eq. (24) are related to the 1D prolate spheroidal functions $\psi_m(t)$ and their corresponding eigenvalues λ_m, which were studied by Slepian and Pollak [32] and Frieden [36]. The eigenfunctions read

$$\zeta_m(t) = \frac{1}{\sqrt{\lambda_m}}\psi_m\Big(t - \frac{T}{2}\Big), \tag{28}$$

with the eigenvalues $\gamma_m = \lambda_m/TW$. Note that $\zeta_m(t)$ and γ_m are purely real valued. Thus $\zeta_m(t)$ are CON over the observation interval $t \in (0, T)$, and any 1D function band limited [32,36] by the time-bandwidth product TW can be expanded by $\zeta_m(t)$.

The derivations of Eqs. (26) and (28) are provided in Appendix A.

E. Spatial mode decomposition

Every component of the aperture field can be expanded by the same spatial mode functions $\xi_p(\mathbf{r})$, conditioned on the bounded space-bandwidth product. Specifically, by Mercer's theorem,

$$\varphi_{0,A}(\mathbf{r}, \mathbf{r}') = a_{0,A}(ab)^2 \sum_p \alpha_p \alpha^*_p \xi^*_p(\mathbf{r})\xi_p(\mathbf{r}'). \tag{29}$$

By a generalized relation similar to Mercer's theorem,

$$\varphi_{j,A}(\mathbf{r}, \mathbf{r}') = a_{j,A}(ab)^2 \sum_{p,q} g^*_p(\mathbf{r}_j) g_q(\mathbf{r}_j) \xi^*_p(\mathbf{r})\xi_q(\mathbf{r}'), \tag{30}$$

$$g_p(\mathbf{r}) = \frac{\alpha^*_p}{b\sqrt{z_p}}\psi_p\Big(\frac{\mathbf{r}}{b}\Big), \tag{31}$$

where α_p are related [31] to λ_p by $\lambda_p = (\beta/2\pi)^2|\alpha_p|^2$.

The modal annihilation operators can be written as

$$\hat{a}_{j,p}(t) = \frac{b}{i\delta_R}\mathcal{E}\hat{A}_{j,O}(t)e^{-i\omega_0 t} g_p(\mathbf{r}_j) e^{ik_0(R + \mathbf{r}_j^2/2R)}, \tag{32}$$

$$\hat{a}_{j,p,m} = \frac{b\mathcal{E}}{i\delta_R} g_p(\mathbf{r}_j) e^{ik_0(R+\mathbf{r}_j^2/2R)} \hat{a}_{j,O,m}, \tag{33}$$

where $\delta_R = \lambda_0 R/a$ is the resolution parameter due to diffraction, and $\hat{a}_{j,O,m} = \int_0^T dt\, \zeta^*_m(t)\hat{A}_{j,O}(t)$ are the annihilation operators of the jth source resulted from the temporal decomposition in the object plane. The amplitude dependence of $\hat{a}_{j,p}(t)$ and $\hat{a}_{j,p,m}$ on $\mathbf{r}_j$ is solely through the functions $g_p(\mathbf{r}_j)$, which are normalized to $|\alpha_p|^2$ over the disk of radius b, and which depend on the two-element vector index $p = (N, n)$. N and n are defined in Slepian's paper [31].

The elements of the coherency matrices are derived as

$$V^{(0)}_{0,p,m,q,n} = \mathcal{N}_{0,A}\nu_p \delta_{pq} \Xi_{0,m,n}, \tag{34}$$

$$V^{(0)}_{j,p,m,q,n} = \frac{(ab)^2}{4\pi R^2} g_p(\mathbf{r}_j) g^*_q(\mathbf{r}_j) V_{j,O,m,n}, \tag{35}$$

$$V_{j,O,m,n} = \mathrm{Tr}(\hat{a}_{j,O,m}\hat{\rho}_j \hat{a}^\dagger_{j,O,n}) = \mathcal{N}_j \Xi_{j,m,n}. \tag{36}$$

The above equations show that the spatial and temporal factors are separated due to the assumption of spectrally pure fields. $\mathbf{V}^{(0)}_j$ in Eq. (35) are not diagonal but Hermitian for spatial mode decomposition, since the mode functions are not the eigenfunctions corresponding to the mutual coherence functions of the point sources. It is thus expected that the multimode excitation from the point sources provides much more information than the single-mode one, as discussed in Ref. [25]. This point will become more clear when the quantum Fisher information matrix is discussed later. In this manner, the problem of measuring multimode Gaussian states of multiple point sources becomes more tractable. Refer to Appendix B for the detailed derivations.

F. Temporal decomposition of Lorentzian spectrum

Although the mode decomposition coefficients can always be calculated numerically in classical optics, it is for mathematical convenience and physical insight to find the analytical expressions. To temporally decompose the point sources, the spectral density function of the background field is assumed to be Eq. (27) to obtain the eigenfunctions in Eq. (28), and that of the point sources are assumed to be the Lorentzian

spectrum [33,38],

$$\chi_j(t-t') = e^{-W|t-t'|}, \tag{37}$$

which is typical of quasimonochromatic sources [39].

In this case, every component of the aperture field can be expanded by the same temporal mode functions $\zeta_m(t)$ in Eq. (28), conditioned on the bounded time-bandwidth product. Again by Mercer's theorem,

$$\chi_0(t-t') = T\sum_m \gamma_m \zeta_m(t)\zeta_m(t'). \tag{38}$$

By a generalized relation similar to Mercer's theorem,

$$\chi_j(t-t') = T\sum_m\sum_n \epsilon_m^{(+)}\epsilon_n^{(-)}\zeta_m(t)\zeta_n(t'), \tag{39}$$

where $\epsilon_m^{(+)} = a_m^{(+)}\sqrt{W\gamma_m}$, and

$$a_m^{(+)} = \frac{1}{\lambda_m}\int_{-T/2}^{T/2} e^{W(t'+T/2)}\psi_m(t')dt', \tag{40}$$

$$a_n^{(-)} = \frac{1}{\lambda_n}\int_{-T/2}^{T/2} e^{-W(t'+T/2)}\psi_n(t')dt'. \tag{41}$$

The elements of the coherency matrices are derived as

$$\Xi_{0,m,n} = T\gamma_m\delta_{mn}, \tag{42}$$

$$\Xi_{j,m,n} = T\epsilon_m^{(-)}\epsilon_n^{(+)}. \tag{43}$$

Note that Ξ_j are not diagonal, since the mode functions are not the eigenfunctions corresponding to the jth temporal mutual coherence function. Refer to Appendix B for the derivations.

III. IMPLEMENTATION

The above mode decompositions can be translated into the physical implementation presented in this section. For simplicity, the physical implementation of the spatial decomposition is discussed in detail, while the temporal one can be similarly realized by a modulation in the time or frequency domain. Firstly, as will be shown shortly, a nonabsorptive polarization- and phase-modulating SLM, a lens, and a PBS are used to act as the mode function multiplier, and the free-space propagation acts as the integration over the aperture. In this manner, the spatial mode decomposition is achieved. Secondly, with two additional lenses, the modal field operators in the image plane and their relation to the modal annihilation operators are derived. This relation provides an effective approach to measuring the modal annihilation operators in the image plane. Finally, the problems of multisource measurement in the image plane and multiparameter retrieval are presented, which enable the determination of the coherency matrices and further that of the multimode density operators.

A. Decomposition of aperture fields

From Eqs. (12) and (26), it can be seen that the aperture fields are multiplied by $\xi_p^*(\mathbf{r})$. Therefore, the spatial mode decomposition can be physically implemented by a three-step scheme [see Fig. 2(a)]. In the first step at the aperture, a nonabsorptive SLM modulates the polarization and phase of the aperture field according to the amplitude and phase

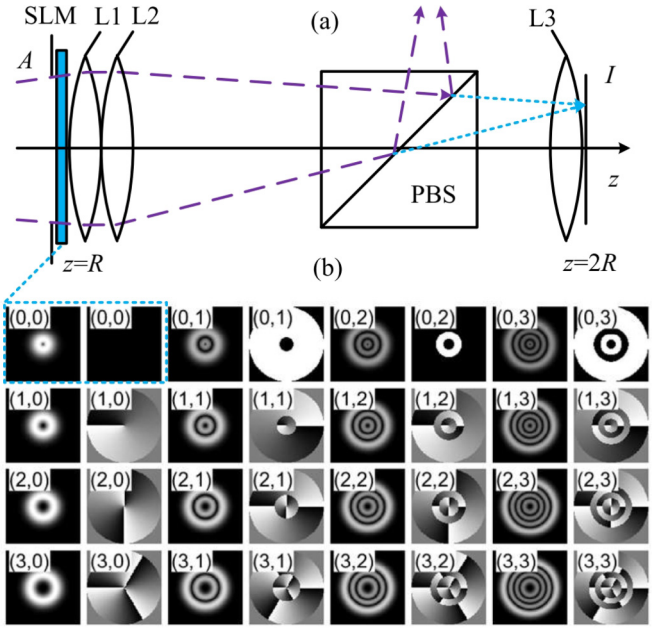

FIG. 2. (a) Implementation of the spatial mode decomposition. The SLM and PBS multiply the aperture field by the function $\psi_p(\mathbf{r}/a)/a\sqrt{z_p}$, and the lens L1 with focal length $f = R$ multiplies the aperture field by $\exp(-i\pi\mathbf{r}^2/\lambda_0 R)$. The other two lenses L2 and L3 with focal length $f = R$ are used to compensate for the phase shifts proportional to $\mathbf{r}^2$. A and I denote the aperture and image plane, respectively. (b) Part of the spatial mode functions $\psi_p(\mathbf{r}/a)/a\sqrt{z_p}$ sequentially loaded onto the SLM. The odd and even columns are the amplitudes and phases, respectively, and the two-element vector indices $p = (N, n)$ are labeled at the upper left corners.

of the function $\psi_p(\mathbf{r}/a)/a\sqrt{z_p}$, respectively. A lens labeled L1 with focal length $f = R$ provides the aperture field with phase retardation according to the function $\exp(-i\pi\mathbf{r}^2/\lambda_0 R)$. In the second step, a PBS transmits the modal field selected by the SLM and reflects the remaining modes. The free-space propagation of the field from the aperture to the transmission port of the PBS is the third step, where the integration over the aperture A takes effect. Figure 2(b) illustrates the spatial mode functions sequentially loaded onto the SLM. These functions are generated through the theory of Slepian [31] and numerically improved by the method of Ref. [40]. The temporal mode functions can similarly be loaded onto the SLM or other modulators. These functions are generated from the theory of Slepian and Pollak [32] and numerically computed through the procedures provided by Ref. [41]. Refer to Appendix E for the numerical calculation of the spatial mode functions.

Two additional lenses with focal length $f = R$ are used to compensate for the phase shifts proportional to $\mathbf{r}^2$. One is placed next to lens L1, and the other is placed against the image plane I. Then, under the pth mode decomposition and related to the jth point source, the spatial modal field operator in the image plane can be expressed as

$$\hat{E}_{j,I,p}(\mathbf{r},t) = -\frac{1}{\delta_R^2}\frac{b}{a}\mathcal{E}\hat{A}_{j,O}(t)e^{-i\omega_0 t}g_p(\mathbf{r}+\mathbf{r}_j) \times \exp\left[ik_0\left(2R+\mathbf{r}_j^2/2R\right)\right], \tag{44}$$

and the process is similar to that described in Fourier optics [42]. The derivation is outlined in Appendix C. This expression indicates that the transverse fields are linearly proportional to $g_p(\mathbf{r}+\mathbf{r}_j)$, which are symmetric or antisymmetric about the points $\mathbf{r}=-\mathbf{r}_j$ given by the geometrical images of the point sources. The symmetry depends on [31] the index N of $p=(N,n)$ through $\exp(iN\theta)$, the azimuthal part of $\psi_p(\mathbf{r}/b)$. The modal field operators satisfy $\hat{E}_{j,I,p}(\mathbf{r}-\mathbf{r}_j,t)=\hat{E}_{j,I,p}(-\mathbf{r}-\mathbf{r}_j,t)$ for even N, and $\hat{E}_{j,I,p}(\mathbf{r}-\mathbf{r}_j,t)=-\hat{E}_{j,I,p}(-\mathbf{r}-\mathbf{r}_j,t)$ for odd N.

Interestingly, it is found that the spatial modal annihilation operators $\hat{a}_{j,p}(t)$ are related to the spatial modal field operators $\hat{E}_{j,I,p}(\mathbf{r},t)$ in the image plane via

$$\hat{a}_{j,p}(t)=i\lambda_0 R\exp(-ik_0R)\hat{E}_{j,I,p}(\mathbf{0},t). \tag{45}$$

Therefore, $\hat{a}_{j,p}(t)$ inherit the symmetry from $\hat{E}_{j,I,p}(\mathbf{r},t)$. Specifically, since $\hat{E}_{j,I,p}(\mathbf{0},t)=\hat{E}_{j,I,p}(-2\mathbf{r}_j,t)$ for even N and $\hat{E}_{j,I,p}(\mathbf{0},t)=-\hat{E}_{j,I,p}(-2\mathbf{r}_j,t)$ for odd N, the spatial modal annihilation operators $\hat{a}_{j,p}(t)$ can be measured at these points other than $\mathbf{r}=\mathbf{0}$. Note that the scale factor is a complex-valued constant for all the modes, which makes the relation very simple for practical use.

It is worthy to point out that the relation of Eq. (45) is a direct result of the spatial propagation of the field through the optical system described above, and therefore applies to any quantum state of the point sources. In other words, this measurement arrangement is universally applicable to any quantum state, and is independent of the mode functions chosen for the decomposition.

It is noted that the above implementation can be seen as an extension of the work of Helstrom [33], where Helstrom used a similar decomposition for the two-hypothesis testing problems so as to detect a circular uniform object against a background of thermal noise. However, it is applied here to handle the multimode field measurement of multiple point sources against the circular uniform background. Furthermore, there are situations where it is advantageous to use a decomposition that makes the fields of point sources multimode, rather than the one that makes the fields single mode. The latter case has been discussed by Helstrom for point sources. The reason is that multimode fields provide much more degrees of freedom for measurements to retrieve the encoded information of the sources.

It is also noted that a similar method of local oscillator (LO) mode scanning was studied theoretically [25] to determine the coherency matrix and the quadrature covariance matrix, and was studied experimentally [43] to distinguish multiple objects. By the scan over the mode indices of the LO, the overlapped object field modes are detected sequentially. What makes the difference of this paper is twofold. Firstly, the scanning mode functions are loaded through the SLM in the aperture. Therefore, it is intrinsically a parallel way for multiobject measurement, whereas the scan of Ref. [43] is in the LO mode and image space. Secondly, all the hardware is optically passive. Thus it inherently has higher fidelity of the object fields and no excess noise commonly seen in practical LO modes. Nonetheless, Ref. [43] is a valid experimental support for the theoretical framework discussed in this paper.

B. Image plane measurement and parameter retrieval

From the image plane operators in Eq. (44), the modal photon flux operators $\hat{N}_{j,I,p}(\mathbf{r},t)=\hat{E}^\dagger_{j,I,p}\hat{E}_{j,I,p}$ read

$$\hat{N}_{j,I,p}(\mathbf{r},t)=\frac{b^2\mathcal{E}^2}{a^2\delta_R^4}|g_p(\mathbf{r}+\mathbf{r}_j)|^2\hat{A}^\dagger_{j,O}(t)\hat{A}_{j,O}(t), \tag{46}$$

and the spatial modal photon rate operators are obtained from Eq. (45) as

$$\hat{a}^\dagger_{j,p}(t)\hat{a}_{j,p}(t)=(\lambda_0R)^2\hat{N}_{j,I,p}(\mathbf{0},t). \tag{47}$$

It is obvious that $\hat{N}_{j,I,p}(\mathbf{r},t)$ and $\hat{a}^\dagger_{j,p}(t)\hat{a}_{j,p}(t)$ are symmetric with respect to the points $\mathbf{r}=-\mathbf{r}_j$, and $\hat{N}_{j,I,p}(-2\mathbf{r}_j,t)=\hat{N}_{j,I,p}(\mathbf{0},t)$. Therefore, the measurements at these point pairs are equivalent.

Since Eq. (44) is the image plane response to a point source located at $\mathbf{r}_j$ in the object plane, the transfer function from the object plane to the image plane can be easily obtained. When the pth mode is selected by the SLM, the spatial mutual coherence function $\varphi_{0,I,p}(\mathbf{r},\mathbf{r}')$ of the background is derived as

$$\varphi_{0,I,p}(\mathbf{r},\mathbf{r}')=a_{0,A}\lambda_p\left[\frac{1}{b^2z_p}\int_O d^2\mathbf{r}_O\psi_p\left(\frac{\mathbf{r}'+\mathbf{r}_O}{b}\right)\times\psi_p^*\left(\frac{\mathbf{r}+\mathbf{r}_O}{b}\right)\right] \tag{48}$$

$$=a_{0,A}(b/\delta_R)^2\int_O d^2\mathbf{r}_O g_p(\mathbf{r}'+\mathbf{r}_O)g_p^*(\mathbf{r}+\mathbf{r}_O). \tag{49}$$

The modal photon flux of the background $N_{0,I,p}(\mathbf{r},t)$ is calculated as $(\hbar\omega_0)^{-1}\varphi_{0,I,p}(\mathbf{r},\mathbf{r})$ (see Appendix C). Physically, the factor $a_{0,A}=\hbar\omega_0N_0/4\pi R^2$ represents the power emitted per unit area of the background and received per unit area of the aperture, as already shown in $\varphi_{0,A}(\mathbf{r},\mathbf{r}')$ at the aperture in Eq. (10). The eigenvalue λ_p accounts for the photon efficiency of the mode, which is inherent due to diffraction discussed in Sec. II B. The expression in the square brackets represents the transverse distribution and is normalized to unity at $\mathbf{r}=\mathbf{r}'=\mathbf{0}$. Meanwhile, $\varphi_{0,I,p}(\mathbf{r},\mathbf{r}')\propto(b/\delta_R)^2$ means that it is proportional to the number of spatial degrees of freedom in the image plane [33]. The scale factor is controlled by the overlap integral of two $g_p(\mathbf{r})$ functions. This phenomenon is similar to the autocorrelation function of the optical transfer function in diffraction theory [35].

To retrieve the parameters of the background and J point sources, it is convenient to start from the modal photon fluxes defined above. Let $N_{0,I,p}(\cdot)$, $N_{j,I,p}(\cdot)$, and $N_{I,p}(\cdot)$ denote the modal photon fluxes of the background, point sources, and measurements in the image plane, respectively. The following equations are established:

$$N_{I,p}(\mathbf{r}'_j,t)=N_{0,I,p}(\mathbf{r}'_j,t;N_0)+\sum_{j=1}^{J}N_{j,I,p}(\mathbf{r}'_j,t;\mathcal{N}_j,\mathbf{r}_j), \tag{50}$$

for a total of more than $3J+1$ locations $\mathbf{r}'_j$ in the image plane set by the measurement procedure. The locations are preferably near the geometrical images of the J point sources

to make the computation more robust to the classical noises and numerical errors. Therefore, in the sense of least-squares error, more than $3J+1$ nonlinear equations are used to solve for $3J+1$ unknowns N_0, $\mathcal{N}_j$, and $\mathbf{r}_j$.

IV. QUANTUM CRAMÉR-RAO BOUND

As the coherency matrices have been obtained, the QFIM and further the QCRB of the parameter estimation error can be derived. In Helstrom's calculations [33,37], the QFIM is derived from a matrix equation, which is complex valued and unstable for direct numerical computation.

Recently, the efforts to find the QFIM and the optimal measurement for the purpose of attaining the QCRB were reported in literature [44–50]. Significant progress has been made for arbitrary Gaussian states through the Bures distance and quantum fidelity, where the statistical moments, i.e., the displacement vectors and covariance matrices, and their derivatives with respect to the parameters are sufficient to compute the QFIM. Via the Bloch-Messiah reduction [51] to obtain the symplectic transformation matrices and symplectic eigenvalues, the symmetric logarithmic derivative and the QFIM [46–49] can be obtained.

In this section, the QCRB for multimode Gaussian states is briefly discussed firstly. Then, the structural significance of the covariance matrices is revealed. Finally, a numerical study of the QCRBs through the proposed theoretical framework is conducted. The localization errors of multiple point sources are taken as an example.

A. Computable QFIM and QCRB

Arranging the modal annihilation and creation operators in the following form provides the displacement vector and covariance matrix needed to completely describe the multimode Gaussian state of the jth point source,

$$\hat{\mathbf{d}}_j^{(c)} = (\hat{a}_1, \hat{a}_2, \ldots, \hat{a}_1^\dagger, \hat{a}_2^\dagger, \ldots)^T, \tag{51}$$

$$\mathbf{d}_j^{(c)} = \langle \hat{\mathbf{d}}_j^{(c)} \rangle = \mathrm{Tr}\big(\hat{\rho}_j \hat{\mathbf{d}}_j^{(c)}\big), \tag{52}$$

$$\mathbf{V}_j^{(c)} = \big\langle \big\{ \big[\hat{\mathbf{d}}_j^{(c)} - \mathbf{d}_j^{(c)}\big], \big[\hat{\mathbf{d}}_j^{(c),\dagger} - \mathbf{d}_j^{(c),\dagger}\big] \big\} \big\rangle, \tag{53}$$

where $\{\hat{\mathbf{d}}_j, \hat{\mathbf{d}}_j^\dagger\}_{l,l'} = \hat{d}_l \hat{d}_{l'}^\dagger + \hat{d}_{l'}^\dagger \hat{d}_l$ is the compact outer product notation [52], the subscript j is omitted in the components, and the subscript transfer $l = (p, m)$ is for notational simplicity. The CCRs in Eq. (13) can be written as

$$\big[\hat{\mathbf{d}}_j^{(c)}, \hat{\mathbf{d}}_j^{(c),\dagger}\big] = \mathbf{K}, \qquad \mathbf{K} = \mathbf{I} \oplus (-\mathbf{I}), \tag{54}$$

where $\mathbf{I}$ is the L-dimensional identity matrix. The symplectic eigenvalues κ_i of $\mathbf{V}_j^{(c)}$ can be computed [52] by taking the absolute value of the usual eigenvalues of the matrix $\mathcal{V}_j = \mathbf{K}\mathbf{V}_j^{(c)}$. A quantum state is pure if all $\kappa_i = 1$; otherwise, it is a mixed state.

The QFIM $H_{j,s,s'}(\boldsymbol{\epsilon})$ for the parameter vector $\boldsymbol{\epsilon}$ for pure and isothermal states is expressed as [47,49,50]

$$H_{j,s,s'}(\boldsymbol{\epsilon}) = \frac{\upsilon^2}{2(1+\upsilon^2)} \mathrm{tr}\big(\mathcal{V}_j^{-1} \partial_s \mathcal{V}_j \mathcal{V}_j^{-1} \partial_{s'} \mathcal{V}_j\big) + 2\partial_s \mathbf{d}_j^{(c),\dagger} \mathbf{V}_j^{(c),-1} \partial_{s'} \mathbf{d}_j^{(c)}, \tag{55}$$

where $\upsilon = 1$ for pure states, $\upsilon > 1$ for isothermal states. ∂_s and $\partial_{s'}$ denote the derivatives with respect to the parameters ϵ_s and $\epsilon_{s'}$, respectively. tr represents matrix trace.

For mixed states, the QFIM can be calculated as [49,50]

$$H_{j,s,s'}(\boldsymbol{\epsilon}) = \frac{1}{2} \sum_{l=1}^{\mathcal{L}} \mathrm{tr}\big(\mathcal{V}_j^{-l} \partial_s \mathcal{V}_j \mathcal{V}_j^{-l} \partial_{s'} \mathcal{V}_j\big) + R_{\mathcal{L},s,s'} + 2\partial_s \mathbf{d}_j^{(c),\dagger} \mathbf{V}_j^{(c),-1} \partial_{s'} \mathbf{d}_j^{(c)}, \tag{56}$$

with the bounded remainder,

$$|R_{\mathcal{L},s,s'}| \leqslant \frac{\sqrt{\mathrm{tr}[(\mathcal{V}_j \partial_s \mathcal{V}_j)^2]} \sqrt{\mathrm{tr}[(\mathcal{V}_j \partial_{s'} \mathcal{V}_j)^2]}}{2\kappa_{\min}^{2\mathcal{L}+2}(\kappa_{\min}^2 - 1)}, \tag{57}$$

where $\lim_{\mathcal{L}\to\infty} \mathbf{R}_\mathcal{L} = \mathbf{0}$, and $\kappa_{\min} = \min\{\kappa_i\}$ is the smallest symplectic eigenvalue of $\mathbf{V}_j^{(c)}$.

The QCRB $Q_j(\epsilon_s)$ is related to the QFIM $H_{j,s,s'}(\boldsymbol{\epsilon})$ via [33,44]

$$Q_j^2(\epsilon_s) = [\mathfrak{N}\mathbf{H}_j(\boldsymbol{\epsilon})]_{s,s}^{-1}, \tag{58}$$

where $\mathfrak{N}$ is the number of independent and identical measurements. And the root-mean-square error of the parameter estimate is bounded by

$$\Delta\epsilon_s \geqslant Q_j(\epsilon_s). \tag{59}$$

B. Structured covariance matrices

The covariance matrices in Eq. (53) can be rewritten into the following structured matrix form, as outlined in Appendix D:

$$\mathbf{V}_j^{(c)} = 2\begin{pmatrix} \frac{1}{2}\mathbf{I} + \mathbf{V}_j^{(0)} & \mathbf{C}_j^{(0)} \\ \mathbf{C}_j^{(0),*} & \frac{1}{2}\mathbf{I} + \mathbf{V}_j^{(0),*} \end{pmatrix} - 2\begin{pmatrix} \mathbf{V}_j^{(d)} & \mathbf{C}_j^{(d)} \\ \mathbf{C}_j^{(d),*} & \mathbf{V}_j^{(d),*} \end{pmatrix}, \tag{60}$$

where the coherency matrices $\mathbf{V}_j^{(0)} = \mathbf{V}_j^{(0),\dagger}$ are defined in Eq. (18) and explicitly given by Eq. (35), and $\mathbf{V}_j^{(d)} = \mathbf{V}_j^{(d),\dagger}$ can be derived directly from the modal annihilation operators in Eq. (33). The fluctuation-related matrices $\mathbf{C}_j^{(0)} = \mathbf{C}_j^{(0),T}$ and $\mathbf{C}_j^{(d)} = \mathbf{C}_j^{(d),T}$ are defined as

$$C_{j,l,l'}^{(0)} = \tfrac{1}{2}\mathrm{Tr}\big(\{\hat{a}_l, \hat{a}_{l'}\}\hat{\rho}_j\big), \tag{61}$$

$$C_{j,l,l'}^{(d)} = \langle \hat{a}_l \rangle \langle \hat{a}_{l'} \rangle, \tag{62}$$

and $C_{j,l,l'}^{(0)} = \mathrm{Tr}(\hat{a}_l \hat{a}_{l'} \hat{\rho}_j)$ for the CCRs of Eq. (13).

The explicit expression for $C_{j,l,l'}^{(0)}$ can be written as

$$C_{j,p,m,q,n}^{(0)} = -(b\mathcal{E}/\delta_R)^2 g_p(\mathbf{r}_j) g_q(\mathbf{r}_j) e^{ik_0(2R + r_j^2/R)} C_{j,O,m,n}, \tag{63}$$

$$C_{j,O,m,n} = \mathrm{Tr}(\hat{\rho}_j \hat{a}_{j,O,m} \hat{a}_{j,O,n}), \tag{64}$$

from the modal annihilation operators in Eq. (33), and $\mathbf{C}_j^{(d)}$ can be derived in a similar way.

Note that Eqs. (33), (35), and (63) are separated into spatial and temporal parts, and the included operators are in the temporal parts. Therefore, the spatial and temporal modes can be treated separately to make the physics more clear, thanks

to the proper choice of the mode functions and the assumption of spectrally pure fields. Furthermore, the multimode structure can be transformed and enhanced for subtle state discrimination. In fact, from Eqs. (55) and (56), the QFIM is proportional to the sum of the matrix traces. When the derivatives with respect to the parameters are appropriate, which are determined by the quantum system, the QFIM is greater for both more modes and higher purity of quantum states. The reason is that the covariance matrices $\mathbf{V}_j^{(c)}$ are positive-definite Hermitian, and the symplectic eigenvalues are lower-bounded by the eigenvalues of pure states. In other words, the QFIM of pure states is greater than that of mixed states of the same type, and the QFIM of pure states with more modes is even greater than that of pure states with fewer modes.

C. Numerical calculation of QCRB

It has been shown that the displacement vectors, covariance matrices, and their derivatives with respect to the parameter vector $\boldsymbol{\epsilon}$ can be derived analytically from the functions $\psi_p(\mathbf{r}_j/b)$ and their derivatives. In the case where $\boldsymbol{\epsilon}$ takes effect through the propagation from the object plane to the aperture plane, it is ready now to calculate the numerical values of the QCRB. Likewise, in the case where $\boldsymbol{\epsilon}$ takes effect through the temporal behavior of the fields, the functions $\psi_m(t)$ come to play the central roles, and the QCRB can be numerically calculated accordingly.

For simplicity, this paper takes the polar coordinates $\mathbf{r}_j = (r_j, \theta_j)^T$ of the point sources as the parameters of this calculation. The fields of the point sources are assumed to be temporally single-mode thermal states, coherent states, or quadrature squeezed states. The corresponding displacement vectors, coherency matrices, and fluctuation-related matrices are given in Appendix D, which can be used for the explicit expressions Eqs. (33), (35), and (63) to calculate the spatially multimode displacement vectors $\mathbf{d}_j^{(c)}$ in Eq. (52) and covariance matrices $\mathbf{V}_j^{(c)}$ in Eq. (53). As can be seen in Appendix D, the derivatives with respect to the parameters $\boldsymbol{\epsilon} = (r_j, \theta_j)^T$ depend on the functions $g_p(\mathbf{r}_j)$, and can be obtained via Eqs. (31), (E1), (E21), and (E22). Finally, the numerical calculation of the QCRBs $Q_j(r_j)$ and $Q_j(\theta_j)$ is completed by Eqs. (55), (56), and (58). For the point sources in the object plane, the temporally single-mode thermal states are treated as mixed states, while the others are treated as pure states.

The configuration parameters are set as follows. The object plane and the aperture are $b = a = 1$ mm in radius, and are $R = 400$ mm apart. With the central wavelength $\lambda_0 = 0.532$ μm, the space-bandwidth product is $\beta = 29.5$, and the resolution parameter due to diffraction is $\delta_R = 0.213$ mm. The maximum spatial mode indices are $P = (N, n)_{\max}$, and $\mathcal{L} = 100$ matrix traces are included for mixed states. The number of independent and identical measurements is $\mathfrak{N} = 1$.

The QCRBs of the estimation errors Δr_j and $\Delta\theta_j$ of the point sources in coherent states at different locations in the object plane are shown in Fig. 3. Overall, the QCRBs are circularly symmetrical and radially nonuniform. Although the distributions of the QCRBs vary with the maximum spatial mode indices $P = (N, n)_{\max}$, the radially intermediate zone has lower bounds than the central zone. This result is quite

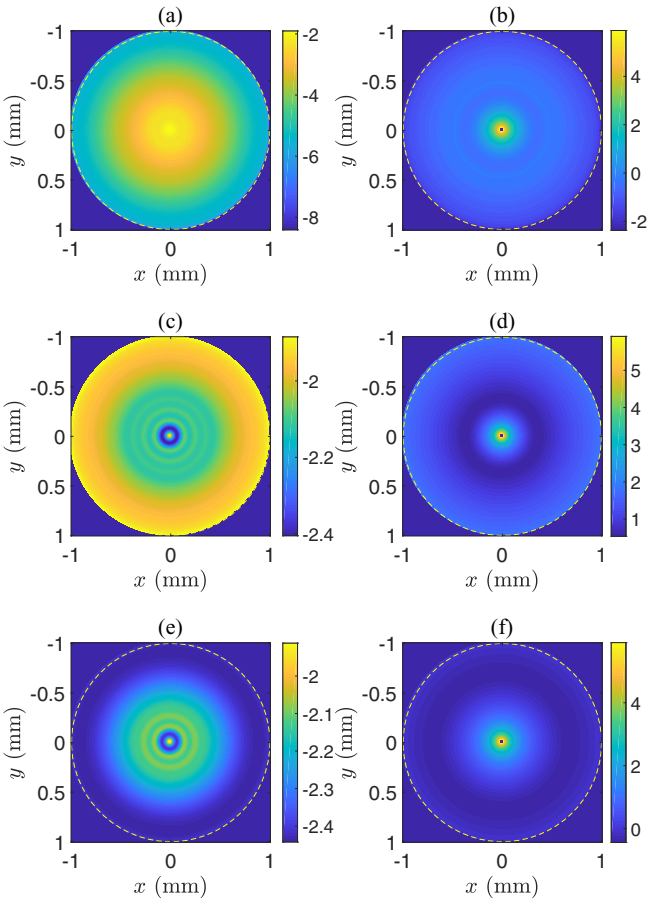

FIG. 3. QCRBs Q_j as functions of the location of the point sources in the object plane. (a), (c), and (e) are for Δr_j, and (b), (d), and (f) are for $\Delta\theta_j$. The maximum spatial mode indices are $(N, n)_{\max} = (9, 9)$ for (a) and (b), (9, 18) for (c) and (d), and (18, 18) for (e) and (f). The units of $Q_j(r_j)$ are millimeters, and that of $Q_j(\theta_j)$ are rad. The point sources are in coherent states, and the mean photon rates $\mathcal{N}_j = 1.0 \times 10^4$. The boundaries of the object plane are marked with yellow circles. To enhance the details, the natural logarithms of Q_j are used.

counterintuitive, since the on-axis point is always in relatively better imaging condition in classical optics. From the expansion of the aperture field in Eq. (11) and the completeness relation in Eq. (A7), the error of mode decomposition approaches zero as $P \to \infty$. Therefore, larger $(N, n)_{\max}$ are preferable, and Figs. 3(e) and 3(f) are more accurate than others. It is also noted that there are singularities at the center of Figs. 3(b), 3(d) and 3(f), where $Q_j(\theta_j)$ approach infinity. This is simple to understand since the azimuthal angle at the center is uncertain mathematically. For thermal states and quadrature squeezed states, the QCRB distributions are similar.

Figure 4 compares the QCRBs for coherent states, thermal states, and quadrature squeezed states, as well as [35] the Rayleigh limit $0.61\delta_R$. In Fig. 4(a), the QCRBs decrease as the mean photon rate $\mathcal{N}_j$ of the point sources increases. The values of coherent states are lower than that of thermal states. The intersection points of the Rayleigh limit with the curves of $Q_j(r_j)$ for coherent states and thermal states appear at $\mathcal{N}_j = 1.0 \times 10^4$ and $\mathcal{N}_j = 1.6 \times 10^4$, respectively. The

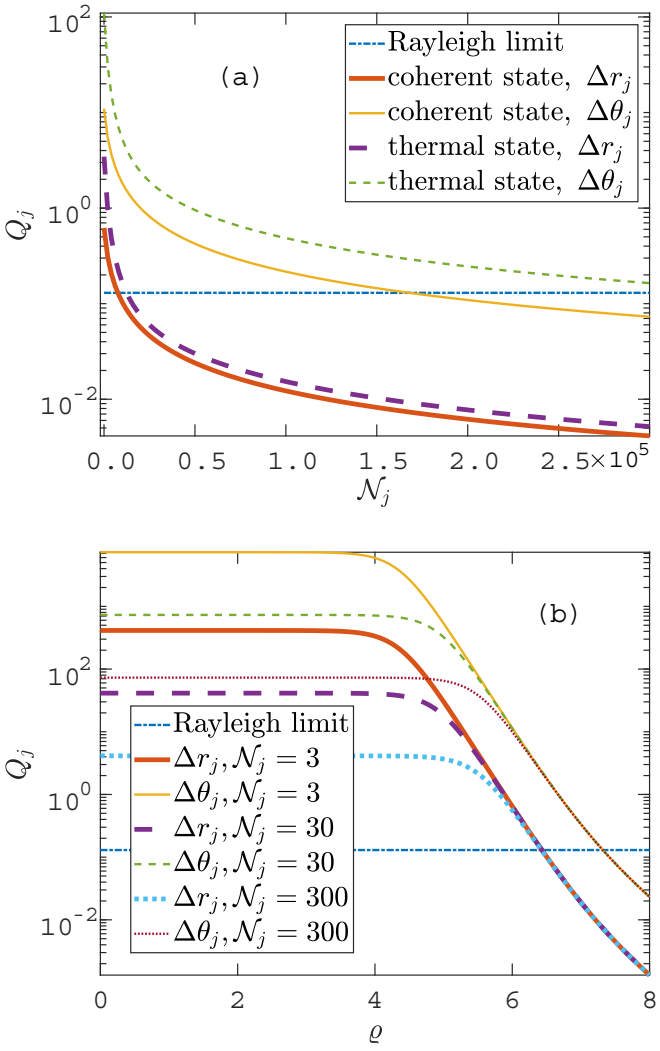

FIG. 4. QCRBs Q_j of Δr_j and $\Delta\theta_j$ as functions of (a) the mean photon rate $\mathcal{N}_j$ and (b) the squeeze parameter ϱ, with $\vartheta = \pi/4$. The units of $Q_j(r_j)$ and the Rayleigh limit are millimeters, and the units of $Q_j(\theta_j)$ are rad. The point source is at the location $r_j = 1/2$ and $\theta_j = 0$ in the object plane. The maximum spatial mode indices are $(N, n)_{\max} = (9, 18)$. For coherent states, $\varrho = 0$.

Rayleigh limit is surpassed once these points are exceeded. For $Q_j(r_j)$ to be 0.013, which is about 1/10 of the Rayleigh limit, the mean photon rates should be $\mathcal{N}_j = 9.6 \times 10^4$ and $\mathcal{N}_j = 1.2 \times 10^5$ for coherent states and thermal states, respectively.

Figure 4(b) shows the dependence of the QCRBs on the squeeze parameter ϱ. For coherent states, $\varrho = 0$, and the curves start with $Q_j(r_j) = 413.02$, 41.30, and 4.13, corresponding to three cases of $\mathcal{N}_j = 3$, 30, and 300, respectively. The difference between coherent and squeezed states is not significant for small values of ϱ. Then they turn downward in the regions around $\varrho \approx 1.88$, 3.06, and 4.19, respectively, and fall off rapidly as ϱ increases beyond those regions. For all three cases, $Q_j(r_j)$ cross the Rayleigh limit at ϱ=6.44 and reach 0.0013 at ϱ=8.0. At ϱ=8.0, $Q_j(r_j)$ are approximately 1% of the Rayleigh limit, or they result in [22] a superresolution factor $S_R = 0.61\delta_R/[Q_j(r_j)] \approx 100$.

Physically, Fig. 4 shows that the Rayleigh limit can always be surpassed by increasing the mean photon rate or squeeze parameter. This confirms the widely recognized fact that the location of a microscopic object can be determined with precision well above the Rayleigh limit, if enough photons are collected, or if squeezed light fields are used. The differences between coherent states and thermal states in Fig. 4(a) are attributed to the differences in the displacement vectors $\langle\hat{a}_{j,O,0}\rangle$ and the fluctuation-related matrices $C_{j,O,0,0}$ [see Eqs. (D9), (D11), (D13), and (D15)]. Specifically, the nonzero $\langle\hat{a}_{j,O,0}\rangle$ and $C_{j,O,0,0}$ of coherent states contribute to the decrease and increase in the QCRB via the QFIM in Eq. (55), respectively. This results in the lower QCRBs for coherent states compared to that of thermal states. The amount of difference depends on $\mathcal{N}_j$. Since the photon number fluctuation of coherent states is less than that of thermal states [38], the above results are consistent with the existing studies. For the curves in Fig. 4(b), the squeeze parameter takes effect entirely through Eqs. (D21) and (D22). An increase in ϱ is equivalent to an increase in $\mathcal{N}_j$ in the manner of $\sinh^2(\varrho)$. Thus the increase in $V_{j,O,0,0}$ and the decrease in the QCRBs are much faster for larger values of ϱ than for smaller values. Meanwhile, $C_{j,O,0,0}$ decreases as ϱ increases in the manner of $(1/2)e^{i\vartheta}\sinh(2\varrho)$, and the decrease in the QCRBs occurs accordingly. Through free-space propagation from the object plane to the aperture, the temporally single-mode fields of point sources become spatially multimode. Therefore, the behavior of the curves is the result of interferences and fluctuation reductions, both of which are intramodal and intermodal.

V. CONCLUDING REMARKS

To solve the imaging and metrology problems with multimode Gaussian states of multiple point sources, quantum coherence theory and quantum diffraction theory have been used to find the field operators and mutual coherence functions at the aperture plane. Considering the circular symmetry of the object plane and aperture, the spatial mode functions are found analytically. The modal annihilation operators and coherency matrices depend on the locations $\mathbf{r}_j$ of the point sources through the functions $g_p(\mathbf{r}_j)$. For a rectangular spectral density function of the background, the temporal mode functions and the decompositions are also found in a similar way.

This multimode decomposition can be physically implemented by a three-step scheme consisting of an SLM, three lenses, and a PBS, which is optically passive and experimentally straightforward. Under this decomposition, the spatial modal annihilation operators are related to the spatial modal field operators in the image plane by a simple complex-valued scale factor. This relation is independent of the mode functions and quantum states of the field. Under the pth mode decomposition and by the photon counting arranged in the image plane, a set of equations can be established to retrieve the unknown parameters of the background and point sources.

Last but not the least, the quantum Fisher information matrix and quantum Cramér-Rao bounds have been discussed and numerically calculated. Interestingly, for coherent states, the numerical calculation shows that the bound in the radially intermediate zone of the object plane is lower than that in the

central area, which is quite counterintuitive, since the on-axis point is always in relatively better imaging condition in classical optics. With large mean photon rates, the well-known Rayleigh limit can always be surpassed by thermal states, coherent states, and quadrature squeezed states. Furthermore, the advantage of quadrature squeezed states is not significant until the squeeze parameter is large enough, which must be taken into account in terms of the practical measurement cost.

As far as the application is concerned, the theory presented in this paper is applicable to the general cases of far-field imaging and parameter estimation, such as microscopy, quantum tomography, and quantum optical computing. Obviously, with minor modification, the theory can also be applied to astronomy, remote sensing, and free-space quantum communication.

ACKNOWLEDGMENTS

We would like to acknowledge Prof. J.K. Liao for helpful discussions.

APPENDIX A: DERIVATION OF THE SPATIAL AND TEMPORAL MODE FUNCTIONS

1. Spatial mode functions

The derivation of the spatial mode functions is basically by comparing the defining integral equation studied by Slepian [31] with the defining integral equation, Eq. (23), where the spatial mutual coherence function of the background Eq. (10) is used. This process is similar to that of Helstrom [37].

Let $\mathbf{r} = a\mathbf{x}$, $\mathbf{r}' = a\mathbf{y}$, and $\mathbf{r}'' = b\mathbf{z}$. Rewrite Eq. (10) as

$$\varphi_{0,A}(\mathbf{r},\mathbf{r}') = \frac{\pi\hbar\omega_0 N_0}{k_0^2 a^2}\exp\left[i\frac{\pi a^2}{\lambda_0 R}\left(\mathbf{y}^2-\mathbf{x}^2\right)\right]K_c(\mathbf{x}-\mathbf{y}), \tag{A1}$$

$$K_c(\mathbf{x}) = \left(\frac{\beta}{2\pi}\right)^2\int_{O_1} d^2\mathbf{z}\exp(i\beta\mathbf{x}\cdot\mathbf{z}), \tag{A2}$$

where $\beta = k_0 ab/R$, and O_1 is a unit-radius disk in the object plane. Substituting Eq. (A1) into Eq. (23) results in

$$\frac{1}{4}\beta^2\nu_p\left[\xi_p(a\mathbf{y})\exp\left(-i\frac{\pi a^2}{\lambda_0 R}\mathbf{y}^2\right)\right] = \int_{A_1} d^2\mathbf{x}\,K_c(\mathbf{x}-\mathbf{y})\left[\xi_p(a\mathbf{x})\exp\left(-i\frac{\pi a^2}{\lambda_0 R}\mathbf{x}^2\right)\right], \tag{A3}$$

where A_1 is a unit-radius disk in the aperture plane. Taking the conjugate of the integral equations in Eqs. (12)–(14) of Ref. [31], and exchanging the positions of $\mathbf{x}$ and $\mathbf{y}$, one obtains

$$\lambda_{N,n}\psi^*_{N,n}(\mathbf{y}) = \int_{A_1} d^2\mathbf{x}\,K_c(\mathbf{x}-\mathbf{y})\psi^*_{N,n}(\mathbf{x}). \tag{A4}$$

Then by comparing Eq. (A3) with Eq. (A4) one finds that

$$\xi_p(a\mathbf{x})\exp\left(-i\frac{\pi a^2}{\lambda_0 R}\mathbf{x}^2\right) = \psi^*_{N,n}(\mathbf{x}), \tag{A5}$$

and $\nu_p = 4\lambda_{N,n}/\beta^2$, with $p = (N,n)$ as the notational transfer. Since $\psi_{N,n}(\mathbf{x})$ in Ref. [31] is not normalized over the unit-radius disk A_1, it is normalized here and delivers $\xi_p(\mathbf{r})$ in Eq. (26).

The orthonormality of $\xi_p(\mathbf{r})$ can be established by the fact that

$$\begin{aligned}\int_A d^2\mathbf{r}\,\xi^*_p(\mathbf{r})\xi_q(\mathbf{r}) &= \int_A d^2\mathbf{r}\frac{1}{a\sqrt{z_p}}\psi_p\left(\frac{\mathbf{r}}{a}\right)\frac{1}{a\sqrt{z_q}}\psi^*_q\left(\frac{\mathbf{r}}{a}\right)\\ &= (1/z_p)\int_{A_1} d^2\mathbf{x}\,\psi_p(\mathbf{x})\psi^*_q(\mathbf{x})\\ &= \delta_{pq},\end{aligned} \tag{A6}$$

and the completeness relation can be derived similarly to Ref. [36] as

$$\sum_{p=0}^{\infty}\xi^*_p(\mathbf{r})\xi_p(\mathbf{r}') = \delta(\mathbf{r}-\mathbf{r}'). \tag{A7}$$

2. Temporal mode functions

For the spectral density function $X_j(\omega)$ in Eq. (27), the temporal mutual coherence function can be expressed as [33]

$$\begin{aligned}\chi_j(t-t') &= (1/2\pi)\int_{-\pi W}^{\pi W} d\omega\,X_j(\omega)e^{-i\omega(t-t')}\\ &= \frac{\sin[\pi W(t-t')]}{\pi W(t-t')}.\end{aligned} \tag{A8}$$

Substitute this result into Eq. (24), then let $t = \tau + T/2$ and $t' = \tau' + T/2$. After some straightforward calculations, the result is

$$TW\gamma_m\zeta_m\left(\tau'+\frac{T}{2}\right) = \int_{-T/2}^{T/2} d\tau\frac{\sin[\pi W(\tau-\tau')]}{\pi(\tau-\tau')}\zeta_m\left(\tau+\frac{T}{2}\right). \tag{A9}$$

Comparing Eq. (A9) with Eq. (11) of Ref. [32], one finds that

$$\zeta_m\left(\tau+\frac{T}{2}\right) = \psi_m(\tau), \tag{A10}$$

and $\gamma_m = \lambda_m/TW$. The normalization over $(0,T)$ yields Eq. (28).

The orthonormality of $\zeta_m(t)$ can be verified as

$$\begin{aligned}\int_0^T dt\,\zeta_m(t)\zeta_n(t) &= \int_0^T dt\frac{1}{\sqrt{\lambda_m}}\psi_m\left(t-\frac{T}{2}\right)\frac{1}{\sqrt{\lambda_n}}\psi_n\left(t-\frac{T}{2}\right)\\ &= \delta_{mn},\end{aligned} \tag{A11}$$

and the completeness relation can be shown similarly to Ref. [36] as

$$\sum_{m=0}^{\infty}\zeta_m(t)\zeta_m(t') = \delta(t-t'). \tag{A12}$$

APPENDIX B: SPATIOTEMPORAL MODE DECOMPOSITIONS

In this Appendix, it will be shown that the spatial and temporal mutual coherence functions at the aperture can be

analytically decomposed by common spatial and temporal mode functions. This allows the modal annihilation operators and coherency matrices to be explicitly expressed by the experimentally determinable quantities.

1. Decomposition of the mutual coherence functions of the background

The mode functions $\xi_p(\mathbf{r})$ in Eq. (26) and the corresponding eigenvalues $\nu_p = 4\lambda_p/\beta^2$ are the solutions to the eigenvalue problem in Eq. (23), when $\varphi_{0,A}(\mathbf{r},\mathbf{r}')$ is included in the kernel function. By Mercer's theorem or the completeness relation in Eq. (A7), one obtains

$$\frac{1}{\hbar\omega_0\mathcal{N}_{0,A}}\varphi_{0,A}(\mathbf{r},\mathbf{r}') = \sum_p \nu_p\xi_p^*(\mathbf{r})\xi_p(\mathbf{r}'). \tag{B1}$$

This leads to Eq. (29) as

$$\begin{aligned}\varphi_{0,A}(\mathbf{r},\mathbf{r}') &= \frac{4\hbar\omega_0\mathcal{N}_{0,A}}{\beta^2}\sum_p \lambda_p\xi_p^*(\mathbf{r})\xi_p(\mathbf{r}')\\ &= \frac{4\hbar\omega_0\mathcal{N}_{0,A}}{\beta^2}\sum_p \left(\frac{\beta}{2\pi}\right)^2\alpha_p\alpha_p^*\xi_p^*(\mathbf{r})\xi_p(\mathbf{r}')\\ &= \frac{\hbar\omega_0 N_0(ab)^2}{4\pi R^2}\sum_p \alpha_p\alpha_p^*\xi_p^*(\mathbf{r})\xi_p(\mathbf{r}')\\ &= a_{0,A}(ab)^2\sum_p \alpha_p\alpha_p^*\xi_p^*(\mathbf{r})\xi_p(\mathbf{r}'),\end{aligned} \tag{B2}$$

where $\lambda_p = (\beta/2\pi)^2|\alpha_p|^2$, $\mathcal{N}_{0A} = N_0(\pi ab)^2/4\pi R^2$, and $a_{0,A} = \hbar\omega_0 N_0/4\pi R^2$.

From $\chi_0(t-t')$ in Eqs. (27) and (A8), according to Eq. (24) and Mercer's theorem, or by the completeness relation in Eq. (A12), the relation in Eq. (38) is easily obtained.

2. Decomposition of the mutual coherence functions of the point sources

To derive the relation in Eq. (30), the following identity can be proven first:

$$\exp(-i\beta\mathbf{x}\cdot\mathbf{y}) = \sum_p \frac{\alpha_p^*}{z_p}\psi_p^*(\mathbf{y})\psi_p(\mathbf{x}). \tag{B3}$$

Proof. From the defining integral equation Eq. (15) of Ref. [31], and with notational change, it is found that

$$\alpha_p\psi_p(\mathbf{x}) = \int_{A_1} d^2\mathbf{y}\exp(i\beta\mathbf{x}\cdot\mathbf{y})\psi_p(\mathbf{y}), \tag{B4}$$

$$\alpha_p^*\psi_p(\mathbf{x}) = \int_{A_1} d^2\mathbf{y}\exp(-i\beta\mathbf{x}\cdot\mathbf{y})\psi_p(\mathbf{y}), \tag{B5}$$

where $p=(N,n)$, $\alpha_{N,n} = i^N 2\pi b_{N,n}$, and $b_{N,n}$ is real. For all $f(\mathbf{y})$ band limited by β, $f(\mathbf{y}) = \sum_p f_p\psi_p(\mathbf{y})$, where $f_p = (1/z_p)\int_{A_1} d^2\mathbf{y}\,\psi_p^*(\mathbf{y})f(\mathbf{y})$. It is simple to show that

$$\begin{aligned}&\int_{A_1} d^2\mathbf{y}\exp(-i\beta\mathbf{x}\cdot\mathbf{y})f(\mathbf{y})\\ &= \sum_p f_p\int_{A_1} d^2\mathbf{y}\exp(-i\beta\mathbf{x}\cdot\mathbf{y})\psi_p(\mathbf{y})\\ &= \sum_p \frac{1}{z_p}\int_{A_1} d^2\mathbf{y}\psi_p^*(\mathbf{y})f(\mathbf{y})\alpha_p^*\psi_p(\mathbf{x})\\ &= \int_{A_1} d^2\mathbf{y}\,f(\mathbf{y})\sum_p \frac{\alpha_p^*}{z_p}\psi_p^*(\mathbf{y})\psi_p(\mathbf{x}).\end{aligned} \tag{B6}$$

Since the above equalities hold for any band-limited function $f(\mathbf{y})$, they deliver Eq. (B3). ■

By Eq. (B3), the factor $\exp[i(k_0/R)(\mathbf{r}-\mathbf{r}')\cdot\mathbf{r}_j]$ in Eq. (9) of $\varphi_{j,A}(\mathbf{r},\mathbf{r}')$, can be rearranged as

$$\begin{aligned}\exp\left[i\frac{k_0}{R}(\mathbf{r}-\mathbf{r}')\cdot\mathbf{r}_j\right] &= \exp(i\beta\mathbf{x}\cdot\mathbf{z}_j)\exp(-i\beta\mathbf{y}\cdot\mathbf{z}_j)\\ &= \sum_{p,q}\frac{\alpha_p\alpha_q^*}{z_p z_q}\psi_p^*(\mathbf{z}_j)\psi_q(\mathbf{z}_j)\psi_p(\mathbf{x})\psi_q^*(\mathbf{y}),\end{aligned} \tag{B7}$$

with $\mathbf{r} = a\mathbf{x}$, $\mathbf{r}' = a\mathbf{y}$, and $\mathbf{r}_j = b\mathbf{z}_j$. Then Eq. (9) becomes

$$\begin{aligned}\varphi_{j,A}(\mathbf{r},\mathbf{r}') &= a_{j,A}\exp\left[i\frac{\pi}{\lambda_0 R}\left(\mathbf{r}'^2-\mathbf{r}^2\right)\right]\\ &\quad\times\sum_{p,q}\frac{\alpha_p\alpha_q^*}{z_p z_q}\psi_p^*(\mathbf{z}_j)\psi_q(\mathbf{z}_j)\psi_p(\mathbf{x})\psi_q^*(\mathbf{y})\\ &= a_{j,A}(ab)^2\sum_{p,q}\frac{\alpha_p}{b\sqrt{z_p}}\psi_p^*\left(\frac{\mathbf{r}_j}{b}\right)\frac{\alpha_q^*}{b\sqrt{z_q}}\psi_q\left(\frac{\mathbf{r}_j}{b}\right)\\ &\quad\times\left[\frac{\psi_p(\mathbf{x})}{a\sqrt{z_p}}\exp\left(-i\frac{\pi}{\lambda_0 R}\mathbf{r}^2\right)\right]\\ &\quad\times\left[\frac{\psi_q^*(\mathbf{y})}{a\sqrt{z_q}}\exp\left(i\frac{\pi}{\lambda_0 R}\mathbf{r}'^2\right)\right]\\ &= a_{j,A}(ab)^2\sum_{p,q} g_p^*(\mathbf{r}_j)g_q(\mathbf{r}_j)\xi_p^*(\mathbf{r})\xi_q(\mathbf{r}'),\end{aligned} \tag{B8}$$

where

$$g_p(\mathbf{r}) = \frac{\alpha_p^*}{b\sqrt{z_p}}\psi_p\left(\frac{\mathbf{r}}{b}\right). \tag{B9}$$

Equation (30) is thus obtained. With $\psi_p(\mathbf{r})$ in Eq. (E1), the symmetry of $g_p(\mathbf{r})$ depends on the factor $\exp(iN\theta)$. Specifically, $g_p(\mathbf{r})$ is even for even N and odd for odd N.

The following identity is needed to derive the temporal part in Eq. (39):

$$e^{W(t-t')} = \sum_{m,n} a_m^{(+)}a_n^{(-)}\psi_m\left(t-\frac{T}{2}\right)\psi_n\left(t'-\frac{T}{2}\right), \tag{B10}$$

with $a_m^{(+)}$ and $a_n^{(-)}$ defined in Eqs. (40) and (41).

Proof. For all $g(t)$ band limited by the time-bandwidth product TW, $g(t) = \sum_m g_m\psi_m(t)$, where $\psi_m(t)$ are the 1D prolate spheroidal functions on $(-T/2, T/2)$, and were studied by Slepian and Pollak [32]. Also e^{Wt} and e^{-Wt} are band limited over the interval $(0,T)$, and can be expanded by $\psi_m(t-T/2)$ with the expansion coefficients given in Eqs. (40) and (41). Therefore, Eq. (B10) is obtained as the product of e^{Wt} and $e^{-Wt'}$. ■

By the temporal mode functions in Eq. (28) and the eigenvalues, Eq. (B10) can be further transformed into

$$e^{W(t-t')} = T\sum_{m,n}\left(a_m^{(+)}\sqrt{W\gamma_m}\right)\left(a_n^{(-)}\sqrt{W\gamma_n}\right)\zeta_m(t)\zeta_n(t'), \tag{B11}$$

with $\epsilon_m^{(+)} = a_m^{(+)}\sqrt{W\gamma_m}$, and $\epsilon_n^{(-)} = a_n^{(-)}\sqrt{W\gamma_n}$. By Eq. (37), the explicit expression for $\chi_j(t-t')$ in Eq. (39) is derived.

3. Derivation of the coherency matrices

The coherency matrix of the background $V^{(0)}_{0,p,m,q,n}$ in Eq. (34) is obtained from Eq. (25) with Eq. (42). For the point sources, the spatial factor $I_{j,p,q}$ in Eq. (21) can be extended by using the explicit expression of $\varphi_{j,A}(\mathbf{r},\mathbf{r}')$ in Eq. (30),

$$\begin{aligned} I_{j,p,q} &= \int_A d^2\mathbf{r}'\int_A d^2\mathbf{r}\,\xi_p^*(\mathbf{r}')\xi_q(\mathbf{r}) \\ &\quad\times a_{j,A}(ab)^2\sum_{p',q'} g_{p'}^*(\mathbf{r}_j)g_{q'}(\mathbf{r}_j)\xi_{p'}^*(\mathbf{r})\xi_{q'}(\mathbf{r}') \\ &= a_{j,A}(ab)^2\sum_{p',q'}\left[g_{q'}(\mathbf{r}_j)\int_A d^2\mathbf{r}'\xi_p^*(\mathbf{r}')\xi_{q'}(\mathbf{r}')\right] \\ &\quad\times\left[g_{p'}^*(\mathbf{r}_j)\int_A d^2\mathbf{r}\,\xi_q(\mathbf{r})\xi_{p'}^*(\mathbf{r})\right] \\ &= a_{j,A}(ab)^2\sum\nolimits_{p',q'}[g_{q'}(\mathbf{r}_j)\delta_{pq'}]\left[g_{p'}^*(\mathbf{r}_j)\delta_{qp'}\right] \\ &= a_{j,A}(ab)^2 g_p(\mathbf{r}_j)g_q^*(\mathbf{r}_j). \end{aligned} \tag{B12}$$

In the above derivation, the orthonormality condition Eq. (A6) is used. Thus $V^{(0)}_{j,p,m,q,n}$ in Eq. (35) is obtained.

The temporal factor $\Xi_{j,m,n}$ in Eq. (22) can also be extended by using $\chi_j(t-t')$ in Eq. (39):

$$\begin{aligned} \Xi_{j,m,n} &= \int_0^T dt'\int_0^T dt\,\zeta_m(t')\zeta_n(t)T\sum_{m',n'}\epsilon_{m'}^{(+)}\epsilon_{n'}^{(-)}\zeta_{m'}(t)\zeta_{n'}(t') \\ &= T\sum_{m',n'}\left[\epsilon_{n'}^{(-)}\int_0^T dt'\zeta_m(t')\zeta_{n'}(t')\right] \\ &\quad\times\left[\epsilon_{m'}^{(+)}\int_0^T dt\,\zeta_n(t)\zeta_{m'}(t)\right] \\ &= T\sum\nolimits_{m',n'}(\epsilon_{n'}^{(-)}\delta_{mn'})(\epsilon_{m'}^{(+)}\delta_{nm'}) \\ &= T\epsilon_m^{(-)}\epsilon_n^{(+)}. \end{aligned} \tag{B13}$$

The orthonormality condition Eq. (A11) is used in the above derivation. Thus the elements of the coherency matrices of the point sources are obtained as shown in Eq. (43).

4. Derivation of the modal annihilation operators

To derive the explicit expression for the modal annihilation operators in Eq. (32), substitute the aperture field in Eq. (8) and the spatial mode functions in Eq. (26) into Eq. (12), and perform the spatial integration. One obtains

$$\begin{aligned} \hat{a}_{j,p}(t) &= \frac{1}{i\lambda_0 R}\mathcal{E}\hat{A}_{j,O}(t)e^{-i\omega_0 t}e^{ik_0R} \\ &\quad\times\int_A d^2\mathbf{r}\exp\left[i\frac{\pi}{\lambda_0 R}\left(-\mathbf{r}^2+|\mathbf{r}-\mathbf{r}_j|^2\right)\right]\frac{\psi_p(\mathbf{r}/a)}{a\sqrt{z_p}}. \end{aligned} \tag{B14}$$

The above integral can be rewritten as the defining integral [31] of the eigenfunctions $\psi_p(\mathbf{x})$, as shown in Eq. (B5):

$$\begin{aligned} &a\exp\left(i\frac{\pi}{\lambda_0 R}\mathbf{r}_j^2\right)\int_{A_1} d^2\mathbf{x}\exp(-i\beta\mathbf{x}\cdot\mathbf{z}_j)\frac{\psi_p(\mathbf{x})}{\sqrt{z_p}} \\ &= a\exp\left(i\frac{\pi}{\lambda_0 R}\mathbf{r}_j^2\right)\alpha_p^*\frac{\psi_p(\mathbf{z}_j)}{\sqrt{z_p}} \\ &= ab\exp\left(i\frac{\pi}{\lambda_0 R}\mathbf{r}_j^2\right)g_p(\mathbf{r}_j), \end{aligned} \tag{B15}$$

and $g_p(\mathbf{r})$ is defined in Eq. (B9). By $\delta_R = \lambda_0 R/a$ being the resolution parameter due to diffraction, the explicit expression of the modal annihilation operators in Eq. (32) is finally obtained.

APPENDIX C: IMAGE PLANE FIELDS

1. Spatial modal field operators

Under the spatiotemporal mode decompositions in the aperture, the field operators in the image plane and related to the J point sources can be derived. For clarity, only the spatial mode decompositions are considered here, and the temporal ones are similar and omitted.

By the SLM and PBS, the factor $\psi_p(\mathbf{r}/a)/a\sqrt{z_p}$ of the spatial mode function $\xi_p^*(\mathbf{r})$ from Eq. (26) is modulated onto the field. After the lens L1 of focal length $f = R$, the modulated field of the jth source can be expressed as

$$\begin{aligned} \xi_p^*(\mathbf{r})\hat{E}_{j,A}(\mathbf{r},t) &= \frac{1}{i\lambda_0 Ra}\mathcal{E}\hat{A}_{j,O}(t)e^{-i\omega_0 t}\exp(ik_0R) \\ &\quad\times\exp\left(i\frac{k_0}{2R}\mathbf{r}_j^2\right)\exp\left(-i\frac{k_0}{R}\mathbf{r}\cdot\mathbf{r}_j\right)\frac{\psi_p(\mathbf{r}/a)}{\sqrt{z_p}}. \end{aligned} \tag{C1}$$

With the second lens L2 of focal length $f = R$ arranged immediately after the lens L1, the field is multiplied by $\exp(-ik_0\mathbf{r}^2/2R)$. Then the field propagates through a distance R in free space toward the image plane, which is described by the diffraction integral using the Green's function in Eq. (7). With the lens L2 taken into account, the diffraction integral of the last two factors of Eq. (C1) is

$$\begin{aligned} &\frac{1}{\sqrt{z_p}}\int_A d^2\mathbf{r}'\exp\left(-i\frac{k_0}{R}\mathbf{r}'\cdot\mathbf{r}_j\right)\psi_p\left(\frac{\mathbf{r}'}{a}\right)\exp\left(-i\frac{k_0}{2R}\mathbf{r}'^2\right) \\ &\quad\times\frac{k_0}{i2\pi R}\exp\left(ik_0R+i\frac{k_0}{2R}|\mathbf{r}-\mathbf{r}'|^2\right) \\ &= \frac{k_0}{i2\pi R\sqrt{z_p}}\exp\left(ik_0R+i\frac{k_0}{2R}\mathbf{r}^2\right) \\ &\quad\times\int_A d^2\mathbf{r}'\exp\left[-i\frac{k_0}{R}(\mathbf{r}+\mathbf{r}_j)\cdot\mathbf{r}'\right]\psi_p\left(\frac{\mathbf{r}'}{a}\right). \end{aligned} \tag{C2}$$

The last integral in Eq. (C2) can be rewritten using the eigenvalue problem in Eq. (B5):

$$\begin{aligned}\int_A d^2\mathbf{r}'\exp\left[-i\frac{k_0}{R}(\mathbf{r}+\mathbf{r}_j)\cdot\mathbf{r}'\right]\psi_p\left(\frac{\mathbf{r}'}{a}\right)&=a^2\int_{A_1}d^2\mathbf{x}\exp[-i\beta(\mathbf{y}+\mathbf{z}_j)\cdot\mathbf{x}]\psi_p(\mathbf{x})\\&=a^2\alpha_p^*\psi_p(\mathbf{y}+\mathbf{z}_j)\\&=a^2\alpha_p^*\psi_p\left(\frac{\mathbf{r}+\mathbf{r}_j}{b}\right).\end{aligned}\tag{C3}$$

The field in the image plane before the last lens L3 can be written as

$$\hat{E}_{j,I',p}(\mathbf{r},t)=-\frac{1}{\delta_R^2}\frac{b}{a}\mathcal{E}\hat{A}_{j,O}(t)e^{-i\omega_0 t}g_p(\mathbf{r}+\mathbf{r}_j)\times\exp\left[ik_0\left(2R+\frac{\mathbf{r}_j^2}{2R}+\frac{\mathbf{r}^2}{2R}\right)\right].\tag{C4}$$

On account of the last lens L3 of focal length $f=R$, which multiplies the field with $\exp(-ik_0\mathbf{r}^2/2R)$, the image plane field under the pth spatial mode decomposition is obtained as shown in Eq. (44).

2. Modal transfer function and modal coherence function

From the field operator in Eq. (44), the complex transfer function from the object plane to the image plane under the pth spatial mode decomposition can be written as

$$K_{j,I,p}(\mathbf{r}_O,\mathbf{r})=-\frac{1}{\delta_R^2}\frac{b}{a}g_p(\mathbf{r}+\mathbf{r}_O)\exp\left[ik_0\left(2R+\frac{\mathbf{r}_O^2}{2R}\right)\right].\tag{C5}$$

Accordingly, the spatial mutual coherence function in the image plane can be calculated as

$$\varphi_{j,I,p}(\mathbf{r},\mathbf{r}')=\int_O d^2\mathbf{r}_2' K_{j,I,p}(\mathbf{r}_2',\mathbf{r}')\times\int_O d^2\mathbf{r}_1' K_{j,I,p}^*(\mathbf{r}_1',\mathbf{r})\varphi_{j,O}(\mathbf{r}_1',\mathbf{r}_2').\tag{C6}$$

For the background, substituting Eq. (6) into the above equation, one obtains

$$\begin{aligned}\varphi_{0,I,p}(\mathbf{r},\mathbf{r}')&=a_{0,A}\lambda_p\frac{1}{b^2 z_p}\int_O d^2\mathbf{r}_O\psi_p\left(\frac{\mathbf{r}'+\mathbf{r}_O}{b}\right)\psi_p^*\left(\frac{\mathbf{r}+\mathbf{r}_O}{b}\right)\\&=a_{0,A}\left(\frac{b}{\delta_R}\right)^2\int_O d^2\mathbf{r}_O g_p(\mathbf{r}'+\mathbf{r}_O)g_p^*(\mathbf{r}+\mathbf{r}_O),\end{aligned}\tag{C7}$$

where $(b/\delta_R)^2=(\beta/2\pi)^2$. Thus Eqs. (48) and (49) are obtained.

APPENDIX D: COVARIANCE MATRICES

1. Matrix operations

Starting from the definitions of the displacement vector and covariance matrix in Eqs. (52) and (53), one can show that

$$\mathbf{V}_j^{(c)}=\langle\{\hat{\mathbf{d}}_j^{(c)},\hat{\mathbf{d}}_j^{(c),\dagger}\}\rangle-\left\{\langle\hat{\mathbf{d}}_j^{(c)}\rangle,\langle\hat{\mathbf{d}}_j^{(c)}\rangle^\dagger\right\}.\tag{D1}$$

After a laborious matrix calculation and making use of the CCRs in Eq. (13), one obtains

$$\langle\{\hat{\mathbf{d}}_j^{(c)},\hat{\mathbf{d}}_j^{(c),\dagger}\}\rangle=2\begin{pmatrix}\frac{1}{2}\mathbf{I}+\mathbf{V}_j^{(0)}&\mathbf{C}_j^{(0)}\\\mathbf{C}_j^{(0),*}&\frac{1}{2}\mathbf{I}+\mathbf{V}_j^{(0),*}\end{pmatrix},\tag{D2}$$

$$\left\{\langle\hat{\mathbf{d}}_j^{(c)}\rangle,\langle\hat{\mathbf{d}}_j^{(c)}\rangle^\dagger\right\}=2\begin{pmatrix}\mathbf{V}_j^{(d)}&\mathbf{C}_j^{(d)}\\\mathbf{C}_j^{(d),*}&\mathbf{V}_j^{(d),*}\end{pmatrix},\tag{D3}$$

where the block matrices are derived from Eq. (D1) as

$$\mathbf{I}+2\mathbf{V}_j^{(0)}=\begin{pmatrix}\langle\hat{a}_1\hat{a}_1^\dagger\rangle+\langle\hat{a}_1^\dagger\hat{a}_1\rangle&\langle\hat{a}_1\hat{a}_2^\dagger\rangle+\langle\hat{a}_2^\dagger\hat{a}_1\rangle&\cdots\\\langle\hat{a}_2\hat{a}_1^\dagger\rangle+\langle\hat{a}_1^\dagger\hat{a}_2\rangle&\langle\hat{a}_2\hat{a}_2^\dagger\rangle+\langle\hat{a}_2^\dagger\hat{a}_2\rangle&\cdots\\\vdots&\vdots&\ddots\end{pmatrix},\tag{D4}$$

$$2\mathbf{C}_j^{(0)}=\begin{pmatrix}2\langle\hat{a}_1^2\rangle&\langle\hat{a}_1\hat{a}_2\rangle+\langle\hat{a}_2\hat{a}_1\rangle&\cdots\\\langle\hat{a}_2\hat{a}_1\rangle+\langle\hat{a}_1\hat{a}_2\rangle&2\langle\hat{a}_2^2\rangle&\cdots\\\vdots&\vdots&\ddots\end{pmatrix},\tag{D5}$$

$$2\mathbf{V}_j^{(d)}=2\begin{pmatrix}\langle\hat{a}_1\rangle\langle\hat{a}_1^\dagger\rangle&\langle\hat{a}_1\rangle\langle\hat{a}_2^\dagger\rangle&\cdots\\\langle\hat{a}_2\rangle\langle\hat{a}_1^\dagger\rangle&\langle\hat{a}_2\rangle\langle\hat{a}_2^\dagger\rangle&\cdots\\\vdots&\vdots&\ddots\end{pmatrix},\tag{D6}$$

$$2\mathbf{C}_j^{(d)}=2\begin{pmatrix}\langle\hat{a}_1\rangle^2&\langle\hat{a}_1\rangle\langle\hat{a}_2\rangle&\cdots\\\langle\hat{a}_2\rangle\langle\hat{a}_1\rangle&\langle\hat{a}_2\rangle^2&\cdots\\\vdots&\vdots&\ddots\end{pmatrix}.\tag{D7}$$

Thus Eq. (60) is obtained.

2. Typical single-mode Gaussian states

The displacement vectors, coherency matrices, and fluctuation-related matrices of the single temporal mode thermal states, coherent states, and quadrature squeezed states are calculated here [38]. The subscripts for multimode fields and multiple point sources are retained for consistency.

For thermal states, the density operators read

$$\hat{\rho}_j=\frac{1}{1+\mathcal{N}_j}\sum_{n=0}^{\infty}\left(\frac{\mathcal{N}_j}{1+\mathcal{N}_j}\right)^n|n\rangle\langle n|.\tag{D8}$$

Thus the displacement vectors, coherency matrices, and fluctuation-related matrices are

$$\langle\hat{a}_{j,O,0}\rangle=\mathrm{Tr}(\hat{\rho}_j\hat{a}_{j,O,0})=0,\tag{D9}$$

$$V_{j,O,0,0}=\mathrm{Tr}(\hat{a}_{j,O,0}\hat{\rho}_j\hat{a}_{j,O,0}^\dagger)=\mathcal{N}_j,\tag{D10}$$

$$C_{j,O,0,0}=\mathrm{Tr}(\hat{\rho}_j\hat{a}_{j,O,0}^2)=0.\tag{D11}$$

For coherent states,

$$\hat{\rho}_j=|\alpha\rangle\langle\alpha|,\tag{D12}$$

$$\langle\hat{a}_{j,O,0}\rangle=\alpha_{j,O,0},\tag{D13}$$

$$V_{j,O,0,0}=|\alpha_{j,O,0}|^2=\mathcal{N}_j,\tag{D14}$$

$$C_{j,O,0,0}=\alpha_{j,O,0}^2.\tag{D15}$$

For quadrature squeezed states,

$$\hat{\rho}_j = |\alpha, \varsigma\rangle\langle\alpha, \varsigma|, \tag{D16}$$

$$|\alpha, \varsigma\rangle = \hat{D}(\alpha)\hat{S}(\varsigma)|0\rangle, \tag{D17}$$

with the squeeze operator $\hat{S}(\varsigma)$ and the displacement operator $\hat{D}(\alpha)$ defined as

$$\hat{S}(\varsigma) = \exp[(\varsigma^*\hat{a}^2 - \varsigma\hat{a}^{\dagger 2})/2], \tag{D18}$$

$$\hat{D}(\alpha) = \exp(\alpha\hat{a}^\dagger - \alpha^*\hat{a}), \tag{D19}$$

where $\varsigma = \varrho\, e^{i\vartheta}$, and ϱ is the squeeze parameter. Thus,

$$\langle\hat{a}_{j,O,0}\rangle = \alpha_{j,O,0}, \tag{D20}$$

$$V_{j,O,0,0} = \mathcal{N}_j + \sinh^2(\varrho), \tag{D21}$$

$$C_{j,O,0,0} = \alpha_{j,O,0}^2 - e^{i\vartheta}\sinh(2\varrho)/2. \tag{D22}$$

Finally, the matrices needed to calculate the covariance matrices in Eq. (60) can be written explicitly as

$$\mathbf{V}_j^{(0)} = \frac{(ab)^2}{4\pi R^2}\begin{pmatrix} g_1g_1^* & g_1g_2^* & \cdots \\ g_2g_1^* & g_2g_2^* & \cdots \\ \vdots & \vdots & \ddots \end{pmatrix} V_{j,O,0,0}, \tag{D23}$$

$$\mathbf{V}_j^{(d)} = \frac{b^2\mathcal{E}^2}{\delta_R^2}\begin{pmatrix} g_1g_1^* & g_1g_2^* & \cdots \\ g_2g_1^* & g_2g_2^* & \cdots \\ \vdots & \vdots & \ddots \end{pmatrix} |\langle\hat{a}_{j,O,0}\rangle|^2, \tag{D24}$$

$$\mathbf{C}_j^{(0)} = -\frac{b^2\mathcal{E}^2}{\delta_R^2}\, e^{ik_0(2R+\mathbf{r}_j^2/R)}\begin{pmatrix} g_1g_1 & g_1g_2 & \cdots \\ g_2g_1 & g_2g_2 & \cdots \\ \vdots & \vdots & \ddots \end{pmatrix} C_{j,O,0,0}, \tag{D25}$$

$$\mathbf{C}_j^{(d)} = -\frac{b^2\mathcal{E}^2}{\delta_R^2}\, e^{ik_0(2R+\mathbf{r}_j^2/R)}\begin{pmatrix} g_1g_1 & g_1g_2 & \cdots \\ g_2g_1 & g_2g_2 & \cdots \\ \vdots & \vdots & \ddots \end{pmatrix} \langle\hat{a}_{j,O,0}\rangle^2, \tag{D26}$$

where $g_p(\mathbf{r}_j)$ are written as g_p for notational simplicity.

APPENDIX E: NUMERICAL CALCULATION OF SPATIAL MODE FUNCTIONS

The functions $\psi_p(\mathbf{r})$ needed to define the spatial mode functions $\xi_p(\mathbf{r})$ via Eq. (26) are directly related to the generalized prolate spheroidal functions $\varphi_{N,n}(r)$ studied by Slepian [31],

$$\psi_p(\mathbf{r}) = \psi_{N,n}(r,\theta) = R_{N,n}(r)\exp(iN\theta) = \left(\frac{1}{\sqrt{r}}\right)\varphi_{N,n}(r)\exp(iN\theta) \quad (0 \leqslant r \leqslant 1). \tag{E1}$$

The functions $\varphi_{N,n}(r)$ are real valued and

$$\varphi_{N,n}(r) = \sum_{s=0}^{S} d_s^{(N,n)}(\beta)T_{N,s}(r), \tag{E2}$$

where $S \to \infty$. The functions $T_{N,s}(r)$ are related [31,40] to the Jacobi polynomials $P_s^{(a,b)}(x)$ as

$$T_{N,s}(r) = h_{N,s}\binom{N+s}{s}^{-1} r^{N+1/2}P_s^{(N,0)}(1-2r^2), \tag{E3}$$

$$h_{N,s} = [2(N+2s+1)]^{1/2}\binom{N+s}{s}, \tag{E4}$$

and $T_{N,s}(r)$ are orthonormal as

$$\int_0^1 T_{N,s}(r)T_{N,s'}(r)dr = \delta_{ss'}. \tag{E5}$$

By substituting the above equations into the generalized prolate differential equation with eigenvalue χ, and by using the three-term recursion relation of $P_s^{(a,b)}(x)$, one obtains

$$\vartheta_s^{(1)}d_{s+1}^{(N,n)} + \left(\vartheta_s^{(0)} - \chi\right)d_s^{(N,n)} + \vartheta_s^{(-1)}d_{s-1}^{(N,n)} = 0, \tag{E6}$$

where the dependence on β is omitted for simplicity, and

$$\vartheta_s^{(1)} = \beta^2\gamma_{N,s+1}^{(1)} \quad (s \geqslant 0), \tag{E7}$$

$$\vartheta_s^{(0)} = \kappa_{N,s} + \beta^2\gamma_{N,s}^{(0)} \quad (s \geqslant 0), \tag{E8}$$

$$\vartheta_s^{(-1)} = \beta^2\gamma_{N,s-1}^{(-1)} \quad (s \geqslant 1), \tag{E9}$$

$$\kappa_{N,s} = (N+2s+1/2)(N+2s+3/2), \tag{E10}$$

$$\gamma_{N,s}^{(-1)} = -\frac{(s+N+1)^2}{(2s+N+1)(2s+N+2)}\frac{h_{N,s}}{h_{N,s+1}}, \tag{E11}$$

$$\gamma_{N,s}^{(0)} = \frac{2s(s+1)+N(2s+N+1)}{(2s+N)(2s+N+2)}, \tag{E12}$$

$$\gamma_{N,s}^{(1)} = -\frac{s^2}{(2s+N)(2s+N+1)}\frac{h_{N,s}}{h_{N,s-1}}. \tag{E13}$$

Then one obtains an eigenvalue problem of a tridiagonal matrix,

$$\mathbf{B} = \begin{pmatrix} \vartheta_0^{(0)} & \vartheta_0^{(1)} & 0 & \cdots & 0 & 0 \\ \vartheta_1^{(-1)} & \vartheta_1^{(0)} & \vartheta_1^{(1)} & \cdots & 0 & 0 \\ \vdots & \vdots & \vdots & \ddots & \vdots & \vdots \\ 0 & 0 & 0 & \cdots & \vartheta_{S-1}^{(0)} & \vartheta_{S-1}^{(1)} \\ 0 & 0 & 0 & \cdots & \vartheta_S^{(-1)} & \vartheta_S^{(0)} \end{pmatrix}, \tag{E14}$$

$$\mathbf{d} = \left(d_0^{(N,n)}, d_1^{(N,n)}, \ldots, d_S^{(N,n)}\right)^T, \tag{E15}$$

and

$$\mathbf{B}\mathbf{d} = \chi\mathbf{d}. \tag{E16}$$

The nth eigenvalue $\chi_{N,n}$ and the corresponding eigenvector $\mathbf{d}^{(N,n)}$ of $\mathbf{B}$ are thus found, and $\lambda_{N,n}$ is related to $\mathbf{d}^{(N,n)}$ via [31,36]

$$\lambda_p = \beta\gamma_{N,n}^2, \quad \gamma_{N,n} = \frac{(\beta/2)^{N+1}d_0^{(N,n)}}{(N+1)!\sum_{s=0}^{S}d_s^{(N,n)}}. \tag{E17}$$

Then the eigenvalues corresponding to the spatial mode functions are calculated via $\nu_p = 4\lambda_p/\beta^2$. Substituting the

eigenvector $\mathbf{d}^{(N,n)}$ into Eqs. (E2) and (E1) yields

$$R_{N,n}(r) = \left(\frac{1}{\sqrt{r}}\right)\varphi_{N,n}(r) = \sum_{s=0}^{S} d_s^{(N,n)} h_{N,s} \binom{N+s}{s}^{-1} r^N P_s^{(N,0)}(1-2r^2). \tag{E18}$$

Thanks to the derivative formula of the Jacobi polynomials [53],

$$\frac{d^k}{dx^k}P_s^{(a,b)}(x) = \frac{1}{2^k}(s+a+b+1)_k P_{s-k}^{(a+k,b+k)}(x), \tag{E19}$$

with $(x)_k$ being the Pochhammers symbol [41] defined as

$$(x)_k = x(x+1)\cdots(x+k-1), \tag{E20}$$

the derivative of $R_{N,n}(r)$ with respect to r can be expressed as follows.

For $N = 0$, since $P_0^{(a,b)}(x) = 1$,

$$R'_{N,n}(r) = \sum_{s=1}^{S} d_s^{(0,n)} \sqrt{2(2s+1)}\left[-2r(s+1)P_{s-1}^{(1,1)}(1-2r^2)\right]. \tag{E21}$$

For $N > 0$,

$$R'_{N,n}(r) = d_0^{(N,n)}\sqrt{2(N+1)}Nr^{N-1} + \sum_{s=1}^{S} d_s^{(N,n)} h_{N,s}\binom{N+s}{s}^{-1} \times \left[Nr^{N-1}P_s^{(N,0)}(1-2r^2) - 2r^{N+1}(s+N+1)P_{s-1}^{(N+1,1)}(1-2r^2)\right]. \tag{E22}$$

Finally, by substituting the above equations into Eq. (26) via Eq. (E1), one obtains all the explicit expressions of the spatial mode functions and their derivatives with respect to r. The derivatives with respect to θ can be obtained directly from Eq. (E1).

[1] L. Mandel and E. Wolf, *Optical Coherence and Quantum Optics* (Cambridge University Press, Cambridge, 1995).
[2] R. J. Glauber, Phys. Rev. **130**, 2529 (1963).
[3] R. J. Glauber, Phys. Rev. **131**, 2766 (1963).
[4] M. I. Kolobov, Rev. Mod. Phys. **71**, 1539 (1999).
[5] J. B. Altepeter, E. R. Jeffrey, and P. G. Kwiat, in *Advances in Atomic, Molecular, and Optical Physics*, edited by P. R. Berman and C. C. Lin (Academic, New York, 2005), Vol. 52, pp. 105–159.
[6] A. I. Lvovsky and M. G. Raymer, Rev. Mod. Phys. **81**, 299 (2009).
[7] S. L. Braunstein and P. van Loock, Rev. Mod. Phys. **77**, 513 (2005).
[8] P. Grangier, G. Roger, and A. Aspect, Europhys. Lett. **1**, 173 (1986).
[9] A. Christ, B. Brecht, W. Mauerer, and C. Silberhorn, New J. Phys. **15**, 053038 (2013).
[10] H. P. Yuen and J. H. Shapiro, Opt. Lett. **4**, 334 (1979).
[11] R. Johne, N. A. Gippius, and G. Malpuech, Phys. Rev. B **79**, 155317 (2009).
[12] R. Kolesov, B. Grotz, G. Balasubramanian, R. J. Stöhr, A. A. L. Nicolet, P. R. Hemmer, F. Jelezko, and J. Wrachtrup, Nat. Phys. **5**, 470 (2009).
[13] E. Polino, M. Valeri, N. Spagnolo, and F. Sciarrino, AVS Quantum Sci. **2**, 024703 (2020).
[14] M. Tsang, Phys. Rev. Lett. **102**, 253601 (2009).
[15] M. Tsang, R. Nair, and X.-M. Lu, Phys. Rev. X **6**, 031033 (2016).
[16] C. Lupo and S. Pirandola, Phys. Rev. Lett. **117**, 190802 (2016).
[17] R. Nair and M. Tsang, Phys. Rev. Lett. **117**, 190801 (2016).
[18] F. Yang, R. Nair, M. Tsang, C. Simon, and A. I. Lvovsky, Phys. Rev. A **96**, 063829 (2017).
[19] L. Peng and X.-M. Lu, Phys. Rev. A **103**, 042601 (2021).
[20] C. Oh, S. Zhou, Y. Wong, and L. Jiang, Phys. Rev. Lett. **126**, 120502 (2021).
[21] M. I. Kolobov and C. Fabre, Phys. Rev. Lett. **85**, 3789 (2000).
[22] V. N. Beskrovnyy and M. I. Kolobov, Phys. Rev. A **71**, 043802 (2005).
[23] M. I. Kolobov and V. N. Beskrovnyy, Opt. Commun. **264**, 9 (2006).
[24] V. N. Beskrovny and M. I. Kolobov, Phys. Rev. A **78**, 043824 (2008).
[25] C. Fabre and N. Treps, Rev. Mod. Phys. **92**, 035005 (2020).
[26] H. J. Kimble, Nature (London) **453**, 1023 (2008).
[27] N. C. Menicucci, P. van Loock, M. Gu, C. Weedbrook, T. C. Ralph, and M. A. Nielsen, Phys. Rev. Lett. **97**, 110501 (2006).
[28] S. L. Braunstein, Phys. Rev. A **71**, 055801 (2005).
[29] J. H. Shapiro, IEEE J. Sel. Top. Quantum Electron. **15**, 1547 (2009).
[30] L. Mandel and E. Wolf, Rev. Mod. Phys. **37**, 231 (1965).
[31] D. Slepian, Bell Syst. Tech. J. **43**, 3009 (1964).
[32] D. Slepian and H. O. Pollak, Bell Syst. Tech. J. **40**, 43 (1961).
[33] C. W. Helstrom, *Quantum Detection and Estimation Theory* (Academic, New York, 1976).
[34] C. W. Helstrom, J. Opt. Soc. Am. **59**, 164 (1969).
[35] M. Born and E. Wolf, *Principles of Optics*, 7th ed. (Cambridge University Press, Cambridge, 1999).
[36] B. R. Frieden, in *Progress in Optics*, edited by E. Wolf (Elsevier, New York, 1971), Vol. 9, p. 311.
[37] C. W. Helstrom, J. Opt. Soc. Am. **60**, 233 (1970).
[38] C. C. Gerry and P. L. Knight, *Introductory Quantum Optics* (Cambridge University Press, Cambridge, 2004).
[39] C. W. Helstrom, J. Opt. Soc. Am. **59**, 924 (1969).
[40] Y. Shkolnisky, Appl. Comput. Harmon. Anal. **22**, 235 (2007).
[41] M. Abramowitz and I. A. Stegun, *Handbook of Mathematical Functions with Formulas, Graphs, and Mathematical Tables* (National Bureau of Standards Applied Mathematics, Washington, 1964).
[42] J. W. Goodman, *Introduction to Fourier Optics*, 3rd ed. (McGraw-Hill, New York, 2005).

[43] F. Yang, A. Tashchilina, E. S. Moiseev, C. Simon, and A. I. Lvovsky, Optica **3**, 1148 (2016).
[44] L. Banchi, S. L. Braunstein, and S. Pirandola, Phys. Rev. Lett. **115**, 260501 (2015).
[45] D. Šafránek, Phys. Rev. A **97**, 042322 (2018).
[46] J. Liu, H. Yuan, X.-M. Lu, and X. Wang, J. Phys. A: Math. Theor. **53**, 023001 (2020).
[47] A. Monràs, arXiv:1303.3682.
[48] Y. Gao and H. Lee, Eur. Phys. J. D **68**, 347 (2014).
[49] D. Šafránek, J. Phys. A: Math. Theor. **52**, 035304 (2019).
[50] D. Šafránek, A. Lee, and I. Fuentes, New J. Phys. **17**, 073016 (2015).
[51] C. Weedbrook, S. Pirandola, R. Garcia-Patron, N. J. Cerf, T. C. Ralph, J. H. Shapiro, and S. Lloyd, Rev. Mod. Phys. **84**, 621 (2012).
[52] A. Serafini, *Quantum Continuous Variables: A Primer of Theoretical Methods* (Taylor and Francis, Boca Raton, 2017).
[53] W. Magnus, F. Oberhettinger, and R. P. Soni, *Formulas and Theorems for the Special Functions of Mathematical Physics*, 3rd ed. (Springer-Verlag, Berlin, 1966).